The Kamerlingh Onnes Laboratory

Leiden Institute of Physics

Leiden University

A study towards the roughness of sputtered Au-films

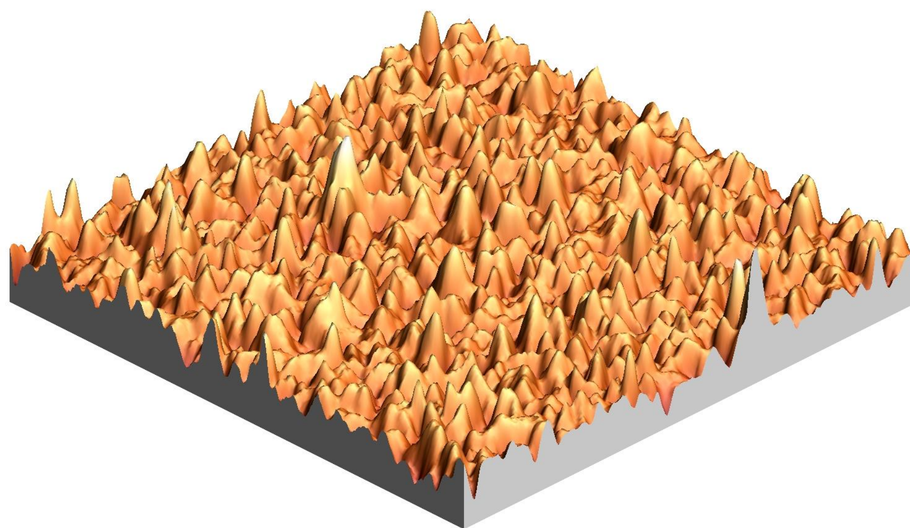

May 1, 2007

A study towards the roughness of sputtered Au-films

Author:	Daan Benjamin Boltje
Supervisors:	Prof. Dr. J. Aarts Ing. R.W.A. Hendrikx
Research conducted at:	'Magnetic and Superconducting Materials' The Kamerlingh Onnes Laboratory Leiden Institute of Physics Niels Bohrweg 2 2333 CA Leiden
HBO Institute	Technische Hogeschool Rijswijk Technische Natuurkunde Lange Kleiweg 80 2288 GK Rijswijk
Period:	February - April 2007
Date:	May 1, 2007

On the cover: 3D topographic AFM image of an Au sample

Preface

Thin film physics is a field of physics where research is continuously progressing under influence of for instance the semiconductor industry and due to the need for research towards superconductivity in thin films.

This internship report covers the research towards the roughness of gold surfaces deposited by sputtering technique. This technique is relatively old, however it still not exactly understood and creating an understanding of this is the second motivator for this research project. To accomplish all of this, a variety of techniques is used including, magnetron and reactive sputtering, atomic force microscopy in different modes and x-ray reflectometry.

The work described within is intended to give an insight in the work done during the three months and hopefully it can also be of assistance for further research towards this particular subject.

Abstract

Thin films are of importance throughout several fields of research and for a variety of applications. In molecular bioelectronics, thin flat gold films are used as a substrate to retain proteins for analysis. The difficulty with this is that the gold films have to be atomically flat otherwise the protein can not be distinguished from the gold surface itself. Atomically flat films can are already deposited, although the understanding of the process itself is not very well understood.

Creating an understanding of the process is the main goal of this project and is addressed by investigating the thickness and roughness as a function of sputtering pressure and the argon-oxygen relation in the sputtering gas. Over 20 samples were made all of them with a different pressure and oxygen concentration. These samples then were analyzed using atomic force microscopy and x-ray reflectometry.

At lower pressure the decrease in film thickness was strongly depended on the oxygen concentration. A decrease of up to 2 nm was found for 2 and 5 mTorr. At higher pressure (10 mTorr) the oxygen concentration did not influence the film thickness, however an overall decrease of up to 3 nm was still found, caused by the higher sputtering pressure. For the films roughness, results were not as definitive due to complications with atomic force microscopy and especially the roughness analysis used.

The pressure and oxygen concentration strongly influence the thickness of the deposited films. However a clear insight of how the roughness of thin gold films depends on pressure and oxygen concentration is not found. This can be done by using other analysis methods for the film roughness and also depositing the films by radio frequency sputtering could provide extra information.

Contents

1 Introduction **1**

2 Thin film deposition & analysis techniques **3**

2.1 Sputtering 3

2.1.1 A brief introduction to the sputtering technique 4

2.1.2 Magnetron sputtering 4

2.1.3 Radio frequency sputtering 7

2.1.4 Reactive sputtering 8

2.1.5 Thin film deposition 9

2.2 Atomic Force Microscopy 11

2.2.1 The basics of atomic force microscopy 11

2.2.2 The piezoelectric scanner 13

2.2.3 AFM cantilevers and probes 15

3 Scope of work **17**

3.1 Thin film deposition 17

3.1.1 The involved parameters 17

3.1.2 ATC-1800 deposition 19

3.1.3 Z-400 deposition 21

3.2 Analysis method 21

3.2.1 Film thickness 21

3.2.2 Film roughness 21

3.2.3 Roughness analysis 23

4 Results **24**

4.1 Thickness of the films 25

4.1.1 XRR measurements 25

4.2 Roughness of the films 25

4.2.1 First AFM set-up 25

4.2.2 Second AFM set-up 28

5 Conclusions & Recommendations **35**

5.1 Conclusions 35

5.2 Recommendations 36

A Au-film process parameters **37**

A.1 02 mTorr samples 37

A.2 02 mTorr 13-04 samples 41

A.3 05 mTorr samples 41

A.4 05 mTorr 13-04 samples 43

A.5 10 mTorr samples March (CM only) 44

A.6 10 mTorr samples April 46

References **49**

List of Figures

2.1 A simple representation of the evaporation and sputtering technique. 3
2.2 Detailed schematic of the effects on surfaces when bombarded by ions. 5
2.3 Effect of electric ($\vec{E}$) and magnetic ($\vec{B}$) fields on a moving electron. 5
2.4 Applied fields and electron motion in a planar magnetron sputtering system. . . . 6
2.5 Formation of pulsating negative sheath on capacitively coupled cathode of RF discharge. 7
2.6 Hysteresis curve of cathode voltage as a function of the reactive gas flow rate at constant discharge current. 8
2.7 Surface processes and growth modes 10
2.8 A schematic representation of the principle of AFM. 11
2.9 The force displayed as a function of the distance between tip and sample. 12
2.10 The different imaging modes (CMAFM, ICMAFM and NCMAFM), schematically displayed. 12
2.11 The effect on piezoelectric materials when a voltage is applied to them. 13
2.12 Piezoelectric tube scanner, sectioned in x, y and z directions. 14
2.13 The voltage characteristic when performing a raster scan with a piezoelectric tube scanner. 14
2.14 Images, made with the scanning electron microscope (SEM), of a silicon cantilever and tip used for ICMAFM. 15
2.15 SEM images of a silicon nitride (for CMAFM) cantilever and tip. 15

3.1 The collision cross-section of the atoms and the swept out volume by that cross-section. 18
3.2 Simple representation of a x-ray measurement. 21
3.3 Example of the same image with and without flatten filter applied. 22

3.4 Two different one-dimensional "surfaces" both zero mean and a total RMS value of 0.5. 23

4.1 Thickness vs. O_2 percentage, measurements done by x-ray reflectometry. 24
4.2 Trace and retrace images of CMAFM on a Z-400 sample. 26
4.3 Final results of the first AFM set-up using CMAFM. 27
4.4 First CMAFM topographic images, made with the second AFM set-up. 28
4.5 Images with tip oscillations due to high gains, the 2D FFT spectra and the resulting images after filtering away the oscillations. 29
4.6 RMS Roughness vs. O_2 percentage, measurements done by AFM. 30
4.7 First results of the topographic images created with ICMAFM. 31
4.8 Example of how grain size is also retraceable in the 2D FFT plot. 31
4.9 RMS roughness vs. O_2 percentage, measurements done by ICMAFM. 32
4.10 AFM images showing the RMS roughness complications. 33

List of Tables

3.1 MoGe adhesion sputter parameters. 20
3.2 Au sputter parameters. 20

A.1 MoGe deposition conditions 37

List of Abbreviations

AFM	Atomic Force Microscopy
CMAFM	Contact Mode Atomic Force Microscopy
FCC	Face-Centered Cubic
FFT	Fast Fourier Transformation
ICMAFM	Intermittent Contact Mode Atomic Force Microscopy
MFP	Mean Free Path
NCMAFM	Non-Contact Mode Atomic Force Microscopy
RF	Radio Frequency
SEM	Scanning Electron Microscope
SPM	Scanning Probe Microscope
STM	Scanning Tunnelling Microscopy
XRR	X-Ray Reflectometry

Chapter 1

Introduction

Thin film deposition techniques were developed and first used in an experimental way at the end of the Nineteenth Century. Sputtering and evaporation were one of these techniques and made it possible to grow very thin films, in the order of nanometers, of any kind of material. The evaporation technology was clearly the favourite technique for this until the late 1960s. Although evaporation had many advantages over sputtering (better vacuum, higher deposition rates) the introduction of radio frequency (RF) and magnetron sputtering variants extended the capabilities of this principle which helped to promote the popularity of sputter deposition.

Due to the simplicity of the physical processes involved and the flexibility for customization, sputtering is not only being used in the scientific, but also in the commercial field. In this field, thin films are used to manufacture sensors, deposit thin antireflection coatings on glass and are also used for packaging. As for the scientists, thin films appear to react very different to phenomena than bulk materials which results in a new field of research. Within this new field thin films are used to perform research towards superconductivity, nanophysics and even scanning probe microscopy on biological systems.

Gold is one of the materials used for researching the material properties at thin film level, [6]-[8] and these thin films are of great importance in for example molecular bioelectronics, where they directly chemisorbed proteins onto thin gold film electrodes. This requires the surface to be atomically flat, which is not as easy as it seems. Although it is known how to make these atomically flat films, the principle behind the process is still not very well understood. There are many ways to create these films, using different methods and sputtering is only one of these. Not only the direct application, but also the fundamental principle of the process is a motivator behind this research project. Recently this problem has already been investigated within the Leiden Institute of Physics, but unfortunately the results were not definitive. Therefore the problem has again been investigated with this report as result.

Outline of report

In order to fully understand and interpret the experiments done, the theory behind this field of research shall be discussed in **chapter 2**. This includes thin film growth and AFM measurements. The devices used, an insight into the involved parameters and the growth process will be discussed in **chapter 3**. Within this chapter the AFM set-up and roughness analysis will also be discussed. The results of the measurements performed will be presented in **chapter 4** and the final chapter, **chapter 5** will include the conclusions and recommendations for further research.

Chapter 2

Thin film deposition & analysis techniques

In this chapter the theory will be discussed in order to create an understanding of the physics behind this field of research. First of all the sputtering technique will be discussed, which will be followed by the theory behind atomic force microscopy (AFM). Most of the theory about sputtering described in this chapter originates from the references [1] and [2] and for AFM, mostly reference [10] is used.

2.1 Sputtering

Sputtering is in essence the same as evaporation (figure 2.1a). Evaporation however, transfers the atoms from the source to substrate by thermal means, whereas sputtering removes source atoms through ion bombardment. The main purpose of sputtering is being able to transfer atoms from a source to a substrate in a controllable way, as shown in figure 2.1b.

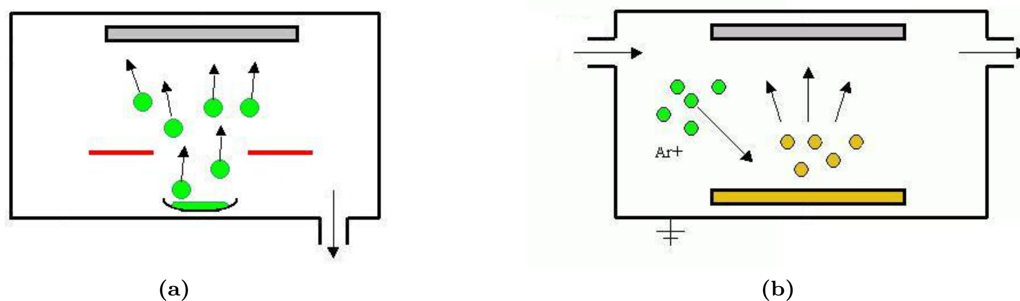

(a) **(b)**

Figure 2.1: A simple representation of the evaporation and sputtering technique. In (*a*) an evaporation set-up is shown, the furnace heats up the material which then evaporates and eventually settles down on the substrate. In (*b*) argon ions bombard the target and remove some target particles which also condense on the substrate.

2.1.1 A brief introduction to the sputtering technique

Deposition by sputtering is carried out in a gas atmosphere with relative high sputtering gas pressure of a few mTorr (1 Pa = 7.5028 mTorr). Also, sputtering is a low temperature process which results in the possibility of depositing thin films on temperature sensitive substrates. Gasses used for sputtering are mainly inert, such as argon. The sputtering process is initiated by applying a negative bias voltage between the target (cathode) and the substrate holder (anode). The electrical field in the chamber separates the argon atoms in argon ions (Ar^+) and free electrons (e^-) therefore the argon gas becomes ionized and a characteristic blue/purple plasma is created. The positive ions in the plasma start bombarding the target as a result of the applied voltage. An incoming argon ion can undergo several processes at the target as shown in figure 2.2, it may

- Undergo elastic collision and be reflected.
- Undergo in-elastic collision and be buried into the target material.
- Produce structural rearrangement in the target material.
- Set up a series of collisions between atoms of the target leading to the ejection of a target atom.

The last possibility is the most important one, because that is what defines sputtering [3]. The process can be thought of as atomic billiards, with the ions (cue ball) striking the neatly arranged target material (billiard balls). This will scatter the target atoms in all directions and thus also in the direction of the substrate. It is this ejected particle that will strike and condense onto the surface under the right conditions and thus is useful for deposition on the substrate. Next to the released target atoms also secondary electrons are emitted which are very important because these enhance the ionizing effect of the argon gas, leading to more ion bombardment and thus to a higher deposition rate.

The general sputtering process as aforementioned can be quite different when the several sputtering variants such as magnetron, RF and reactive sputtering are taken into account. Therefore these will be discussed in the following subsections.

2.1.2 Magnetron sputtering

First described by Penning in 1936 [1], magnetron sputtering has now become one of the widely commercially used sputtering methods. Not only because of the high deposition rates that can be achieved (up to 1 μm/min, [2]), but also because there are many different variations in how to apply the magnetic field etc. The term sputtering magnetron is used for a vast array of devices using electric and magnetic fields. However the term is reserved for devices which satisfy the following so called Penning-conditions [1].

(1) An annular, or annular-like, volume of space threaded by lines of magnetic field which, at either end, intersect surfaces at cathode potential.

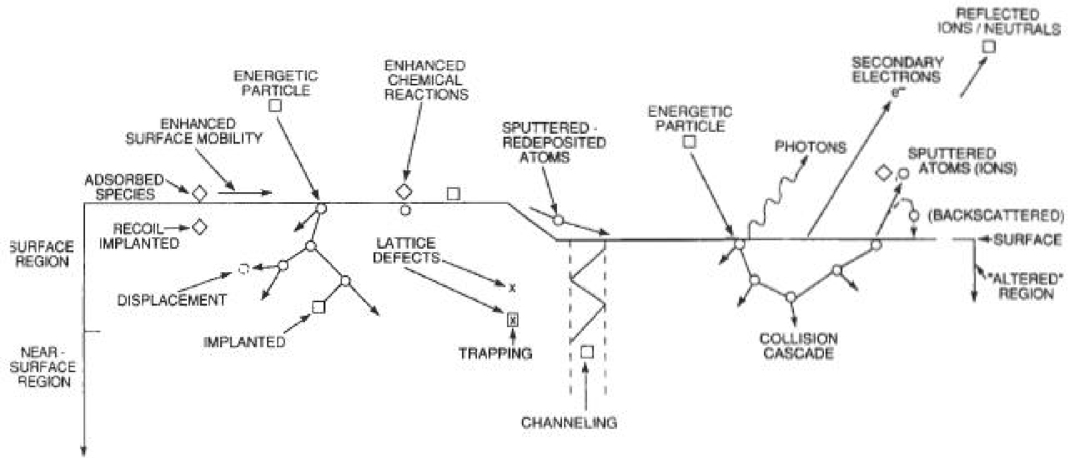

Figure 2.2: Detailed schematic of the effects on surfaces when bombarded by ions. Different particles can be emitted namely: secondary electrons, photons, reflected ions and sputtered atoms. Also an incoming energetic particle (argon ion) can enhance the surface mobility or re-order the surface. Image from [2].

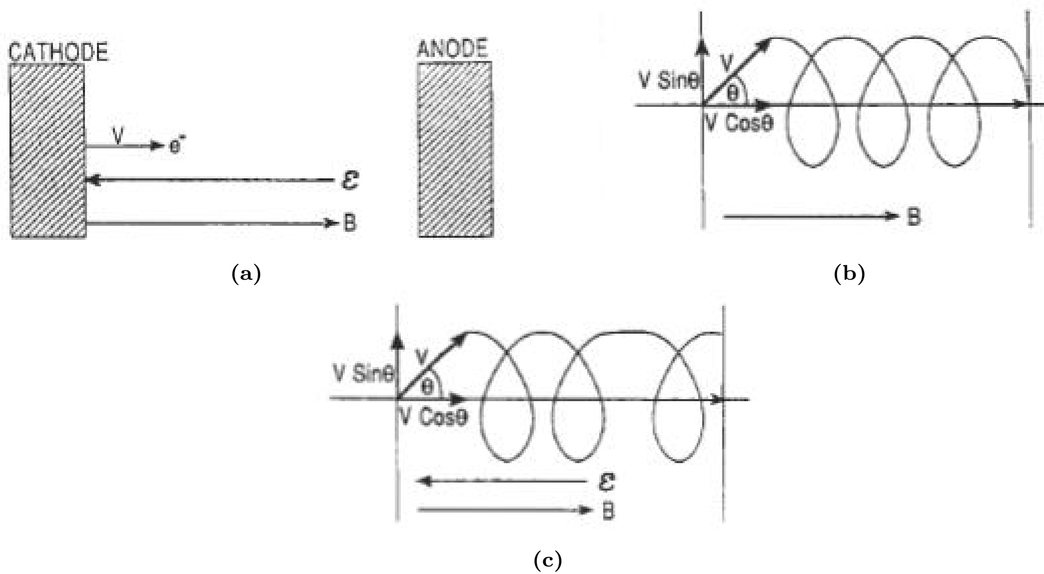

Figure 2.3: Effect of electric ($\vec{E}$) and magnetic ($\vec{B}$) fields on a moving electron. When the electron undergoes a linear trajectory, $\vec{E} \parallel \vec{B}$ $(\theta = 0)$ (a), a helical orbit of constant pitch, $\vec{E} = 0$, $\vec{B} \neq 0$ $(\theta \neq 0)$ (b) and a helical orbit of variable pitch, $\vec{E} \parallel \vec{B}$ $(\theta \neq 0)$ (c). Images from [2].

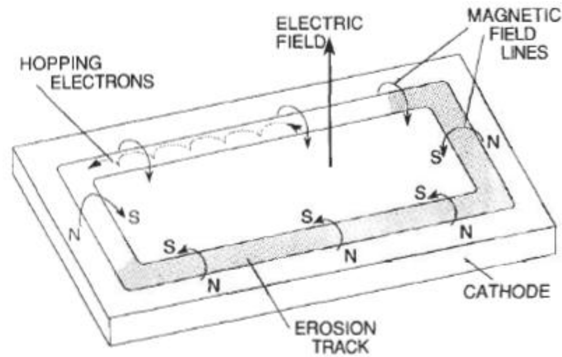

Figure 2.4: Applied fields and electron motion in a planar magnetron sputtering system. Image from [2].

(2) A gaseous glow discharge maintained in the volume by the application of a negative voltage to the cathode surfaces. The dominant voltage drop occurs across positive ion sheaths which form and adhere to the cathode surfaces.

(3) A magnetic field strength high enough to retain the γ-electrons, which are released from the cathode surfaces by ion bombardment, within the volume until a substantial fraction of their energy is lost to ionizing collisions with ambient gas molecules.

(4) A geometry which allows a substantial fraction of the gaseous ions produced in the trap volume to be attracted to, and collected by, the cathode surfaces which delimit the volume. These ions are accelerated by the positive ion sheath at the cathode and cause sputter erosion of cathode material.

Nowadays there is a great variety of sputter magnetrons with very different experimental set-ups and characteristics. Dimensions ranging from a few up to 500 cm are not uncommon with operating voltages ranging from 200 to 900 V.

To understand the sputter magnetron principle it is easy to start with the basics of electromagnetism where the electric, $\vec{E}$ and magnetic, $\vec{B}$ fields play an important role. First figure 2.3a, where the electrons are emitted with $\theta = 0$ and $\vec{E} \parallel \vec{B}$ at the cathode. These electrons are only influenced by the electric field and are accelerated towards the anode in a straight line. Whenever a electron is emitted while $\vec{E} = 0$, $\vec{B} \neq 0$ and with an angle $\theta \neq 0$, the electron is influenced by the Lorentz force and orbits in a circular motion with radius r as shown in figure 2.3b. The result is that the electron makes a helical motion from cathode to anode, with constant velocity. There is one scenario left, figure 2.3c, which only differs 2.3a in the angle at which the electrons are released. Again the electron starts to rotate in a helical motion (as in figure 2.3b), but since the electric field now also has to be considered the electron will also accelerate towards the anode. This results in a helical motion with variable pitch.

Ideally the electrons emitted at the cathode (target) do not reach the anode but are trapped near the target. The helical motion causes the electrons to enlarge the residence time in the plasma, which enhances the collision probability. Placing horseshoe or bar magnets behind the

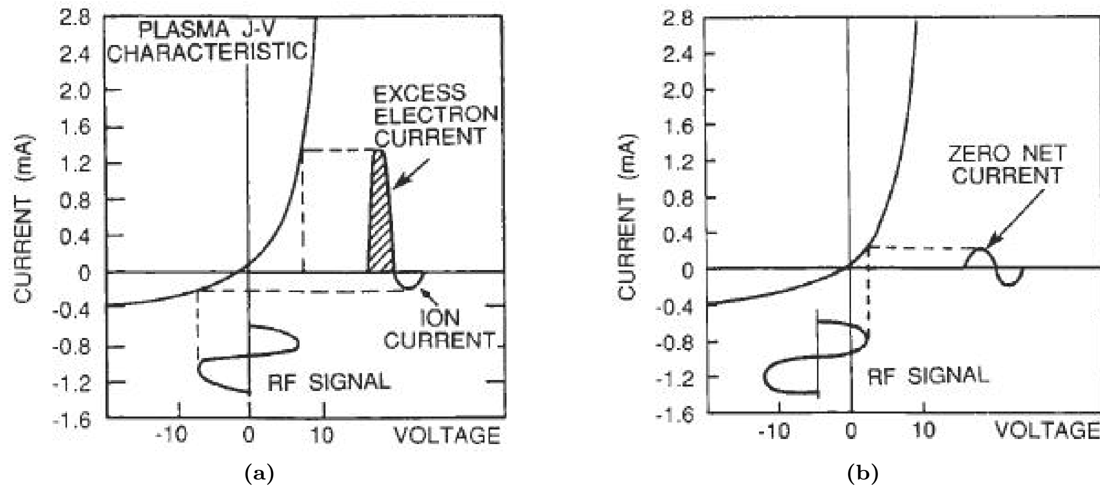

Figure 2.5: Formation of pulsating negative sheath on capacitively coupled cathode of RF discharge. Net current/zero self-bias voltage (*a*). Zero current/nonzero self-bias voltage (*b*). Images from [1].

target, creates a magnetic field parallel to the target and perpendicular to the electric field (figure 2.4). The erosion track forms in that specific way because the ionizing effect of the gas is at a maximum above this erosion track.

2.1.3 Radio frequency sputtering

With the introduction of RF sputtering, it is now also possible to grow insulating thin films. The secret of this, lays in the fact that an AC signal is used instead of a DC signal to create the bias voltage and in the mobility difference of the plasma particles. When this AC signal is applied to the electrodes nothing much happens because the ions and electrons in the plasma are both able to oscillate with the AC signal. When approaching the 50 kHz however two important effects occur (from [2] and [12]), namely:

- The oscillating electrons acquire enough energy to cause ionizing collisions, which removes the need for secondary electron emissions.
- The RF voltage can be coupled through any kind of impedance, thus removing the need of a conductor as electrode.

Therefore RF sputtering makes it possible to sputter any material neglecting its resistance. Although the range from 5 to 30 MHz can be used for sputtering, the Federal Communications Commission (FCC) has reserved 13,56 MHz for plasma processing and is widely used.

Due to the fact that the electrons have a higher mobility than the ions and can follow the periodic change in electrical field quite easily, a negative target bias is created. In figure 2.5b the RF sputtering system is schematically displayed, with the target capacitively coupled to the RF generator. Positively charged electrodes will draw more electron current in one half the RF cycle than the negatively charged electrode will draw ion current in the other half of the RF cycle. This

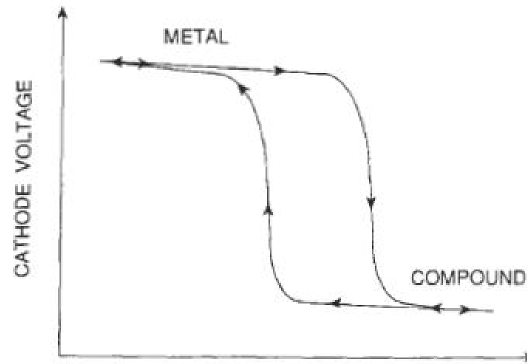

Figure 2.6: Hysteresis curve of cathode voltage as a function of the reactive gas flow rate at constant discharge current. Image from [2].

would result in a net current over the complete cycle if the target was directly coupled to the RF generator. Since this is not the case, no current can flow and therefore the operating point on the characteristic shifts to a negative voltage, the target bias (figure 2.5). This effect occurs on both electrodes which would result in sputtering both the target and the substrate. In order to only sputter the target, the target surface area has to be smaller in respect to the anode. This is easily accomplished since not only the substrate platform serves as anode, also the chamber walls etc. serve as effective anode. The relation between the voltage across the sheath, V_c, and the voltage across the directly coupled electrode, V_d, is given by [1]:

$$\frac{V_c}{V_d} = \left(\frac{A_d}{A_c}\right)^x$$

Where A_d and A_c are the electrode surface areas and the exponent x ranges between 1.5 and 4 which depends on the experimental set-up [2]. So in order to sputter efficiently (minimizing ion bombardment of grounded areas and raising the target sheath potential), a large A_d is required which is simply accomplished by not only grounding the substrate table, but also the walls etc. of the sputtering chamber.

The RF sputtering technique enables sputtering at relatively low pressures of 1-15 mTorr. There are two main reasons for this, first the electrons oscillating at high frequencies cause more collisions resulting in more ionization and secondly none of the electrons are lost because both electrodes are negatively charged, therefore the electrons are reflected back and forth between them.

2.1.4 Reactive sputtering

Mixing a reactive gas, such as oxygen (O_2) into the normal sputtering working gas (Ar) is called reactive sputtering. One of the most commonly reactively sputtered compounds are nitrides and oxides [2]. When sputtering these materials the film is often contaminated by the reactive sputtering gas. Another important aspect of reactive sputtering is the behaviour of the sputtering

gas, while increasing and decreasing the reactive gas flow. In figure 2.6, this is also schematically displayed and shows a hysteresis curve. While keeping the current at a constant value the bias voltage changes when reactive gas flow is increased.

The composition of the plasma created changes when oxygen is also mixed into the sputtering gas. Now there are not only positive argon ions, but also negative oxygen ions which will bombard the anode and thus the substrate as well. This relatively small ion bombardment on the substrate will probably sputter away some substrate or deposited material which will decrease the sputter rate.

2.1.5 Thin film deposition

At this point atoms are being sputtered from the target and need to be deposited on the substrate. This is the most crucial part because the processes which occur at the substrate surface (as shown in figure 2.7a) will influence the formation of the thin film and thus also its roughness. Atoms arriving at the substrate surface will generally move around the surface (diffusion) until they encounter any defects or crystallographic variations on the substrate. These defects will then act as an potential well which the atoms have to overcome. Some will succeed and continue to diffuse around the surface and while doing so some atoms may come across each other and form doublets. More and more atoms arrive, nuclei sizes grow, islands are formed until finally a continuous film is formed. A thin film can form itself into three basic growth modes which are also schematically displayed in figure 2.7b, (from [2] and [12]):

(1) Volmer-Weber (Island)

(2) Frank-van der Merwe (Layer)

(3) Stranski-Krastanov (Layer + Island)

Island growth occurs when the arriving atoms or molecules are more strongly bound to each other than to the substrate. This is often the case when a metal is deposited on an insulator, graphite or mica. When the arriving atoms or molecules are more strongly bound to the substrate than to each other they will form small nucleation sites all over the surface until a thin layer is formed. The following layers will be less tightly bound. This process is called layer growth and is the opposite of island growth. The most important example of this growth mode is single-crystal epitaxial growth of semiconductor films. The intermediate between the two modes discussed is Stranski-Krastanov (S.K.) or layer plus island growth mode. After a few monolayers are formed, the layer growth mode becomes unfavourable and islands start to form. This happens for example when the lattices from substrate and film do not match which often happens in metal-metal or metal-semiconductor systems.

The discussed growth modes only occur when the substrate is not contaminated in any way, because the lattice structure of the substrate material, among other things, influences the growth process. However, when the substrate is contaminated and no characteristic structure is present, the growing film will not be dependant on the substrates surface, which is also being referred to as

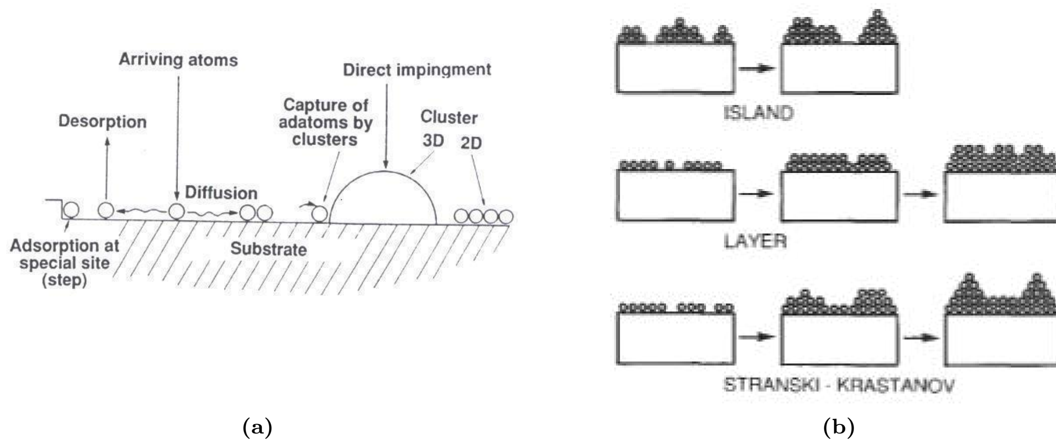

(a) (b)

Figure 2.7: A schematic overview of the processes occurring at the substrate surface (*a*) and the three basic modes of thin film growth (*b*). Images from [1] and [2].

amorphous film growth. Contamination of the substrate is often a result of oxygen binding which forms multiple layers on the substrate.

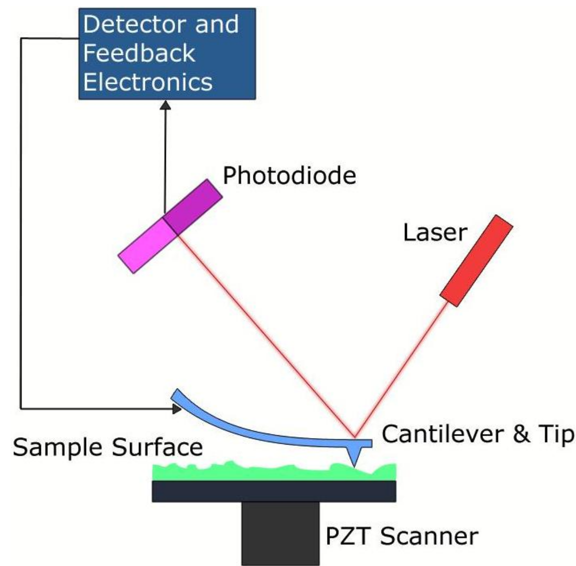

Figure 2.8: A schematic representation of the principle of AFM. Image from [16].

2.2 Atomic Force Microscopy

Within this section the concept of AFM will be discussed. Before G. Binnig, *et al.* proposed the principle of AFM in 1986, there were other methods to measure ultra small forces which relied on electrostatic fields, magnetostatic fields, optical waves and x-rays [10]. It was already possible to measure displacements in the order of even 10^{-4} Åwith capacitance devices. Measuring displacements of 10^{-4} Å, caused by forces as small as 10^{-18} N, is now possible due to the AFM principle. These atomic forces can be measured and thus also surfaces can be imaged with fractions of an Angstrom.

2.2.1 The basics of atomic force microscopy

AFM can achieve such accuracy due to the fact that it measures the microscale cantilevers (which has an ultra small mass) deflection with a laser. The cantilevers are fabricated from silicon (Si) or silicon nitride (Si_3N_4). At the end of this cantilever there is a sharp tip, which is often grown onto the cantilever. The tip, or probe, is used to scan the sample surface and has an end radius of a few nanometer. When the tip approaches the sample surface, the forces which interact between tip and sample lead to a deflection of the cantilever. A laser spot is properly aligned at the end of the cantilever which itself is coated with a reflective material such as gold. This way the slightest deflection is picked up by the photodiode as also shown in figure 2.8. When the tip is close to the sample (the actual distance depends on the AFM mode used) scanning is started, all the movement (x, x and z) is done by the piezoelectric scanner.

There are different imaging modes when using the atomic force microscope. Contact mode AFM (CMAFM) is one of the most commonly used and uses forces (Van der Waals forces, capillary

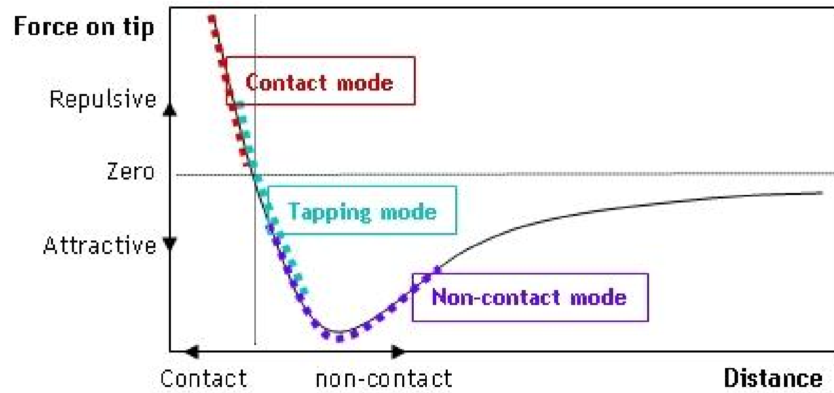

Figure 2.9: The force displayed as a function of the distance between tip and sample. Image from [16].

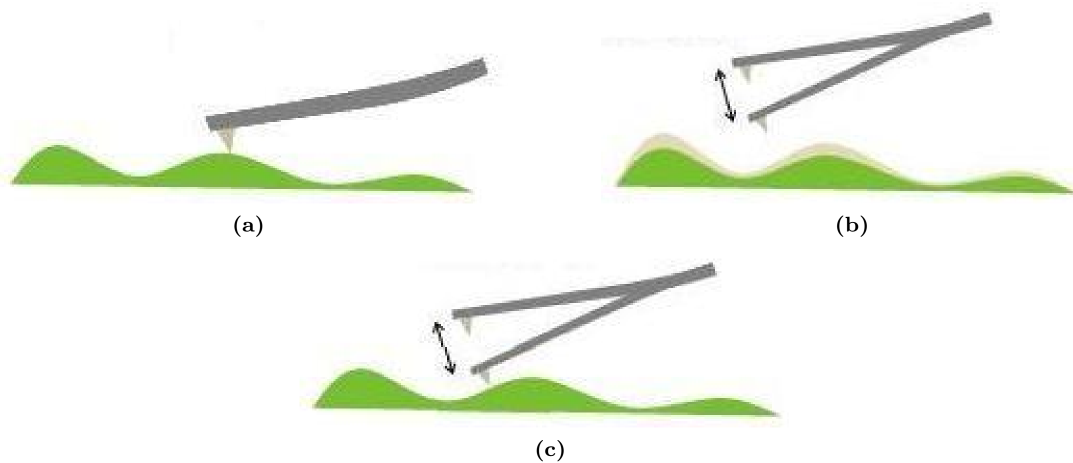

(a) **(b)** **(c)**

Figure 2.10: CMAFM is used to make high resolution images (*a*), ICMAFM where the tip is oscillating and tapping the sample (*b*) and NCMAFM where the tip is also oscillating but not touching the sample (*c*). Images from [16]

.

forces, chemical bonding and electrostatic forces) to map the surface [10]. In figure 2.9 the force is displayed as function of the distance between tip and sample. The left side of the curve is called the repulsive regime which is used for CMAFM. In this mode the repulsive forces are used to map the surface and because these are considerably higher than in non-contact mode AFM (NCMAFM) the imaged surface can easily be damaged by the tip. The distance between tip and sample and thus the force, is kept constant by means of a feedback loop which regulates the piezoelectric scanner. This means that when the tip is encountering a high feature on the surface, the piezoelectric scanner needs to move the sample down in order to keep a constant distance between the tip and sample. Therefore the topographic image created, is made up of the adjustment data and not directly from the deflection of the tip.

In NCMAFM the cantilever is oscillated at a higher frequency than its free resonance (figure 2.10). This all happens while the tip is close to the sample but not touching it. The feedback

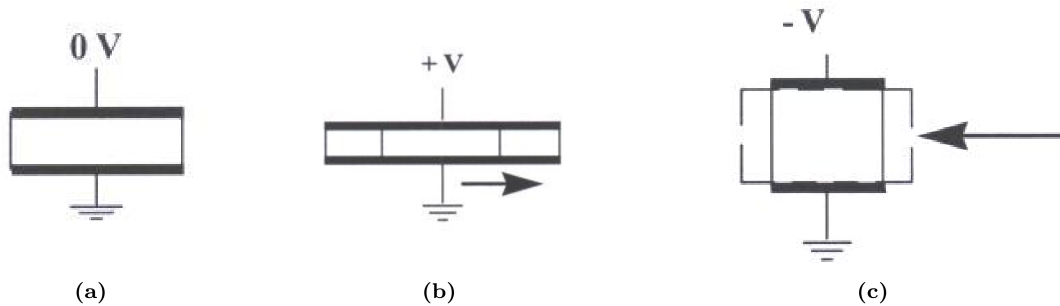

Figure 2.11: The effect on piezoelectric materials when a voltage is applied to them. When no voltage is applied the piezoelectric material is in rest (a). When a positive voltage is applied to the material it extends (*b*) and when an negative voltage is applied to the piezoelectric material it contracts (*a*). Image from [5].

loop is used to maintain an oscillating amplitude setpoint. The attractive forces will lower the resonance frequency and make the oscillation amplitude drop to the setpoint level, when an height difference is encountered.

Intermittent contact mode AFM (ICMAFM), also known as tapping mode AFM, is the intermediate between CMAFM and NCMAFM. This is because the tip literally taps the surface. The tip is closer to the surface than in NCMAFM and still oscillating, see figure 2.10c. An advantage of ICMAFM compared to contact mode is that lateral forces such as drag are almost completely eliminated.

2.2.2 The piezoelectric scanner

In the previous subsection the piezoelectric scanner was briefly mentioned. Since it is such a crucial part for AFM measurements in this subsection it will be discussed more in-depth.

Piezoelectric materials are basically materials that respond to an applied voltage, when applied the material extends or contracts, depending on whether the applied voltage is positive or negative. This is shown also in figure 2.11, where three basic states of piezoelectric materials are shown with or without voltages applied. Thus with three different piezoelectric transducers which independently control the x, y and z direction, the sample can be moved in all directions and measurements can be done [9]. However this method could be improved by using a piezoelectric tube scanner [11], which is shown in figure 2.12. Using this method proves to be easier to fabricate and incorporate into scanning tunnelling microscopy (STM) and AFM set-ups. The different sections of the tube control different directions which results in the ability to manipulate samples with extreme precision in three dimensions. To complete a raster scan the x and y direction have to be manipulated at the same time as in figure 2.13b. This will cause the piezoelectric tube scanner to move as in 2.13a. Separately from the x and y direction, the z direction can also be adjusted as result of the deflection of the cantilever. This all combined results in a working atomic force microscope. There is, however, one small drawback of using piezoelectric scanners, which is hysteresis. Hysteresis is a well know phenomena when using piezoelectric scanners and is caused by differences in the material properties and dimensions of each piezoelectric element, therefore each scanner responds

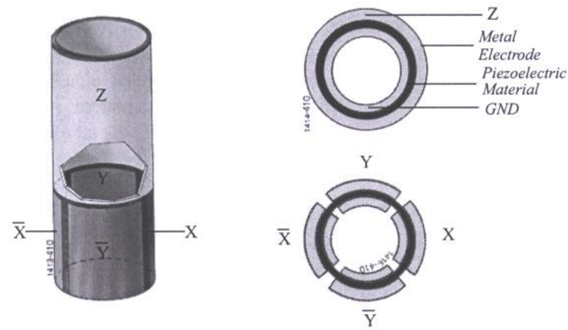

Figure 2.12: Piezoelectric tube scanner, sectioned in x, y and z directions. AC signals are applied in order to move the sample for measuring. DC signals can be used to set offsets. Image from [5].

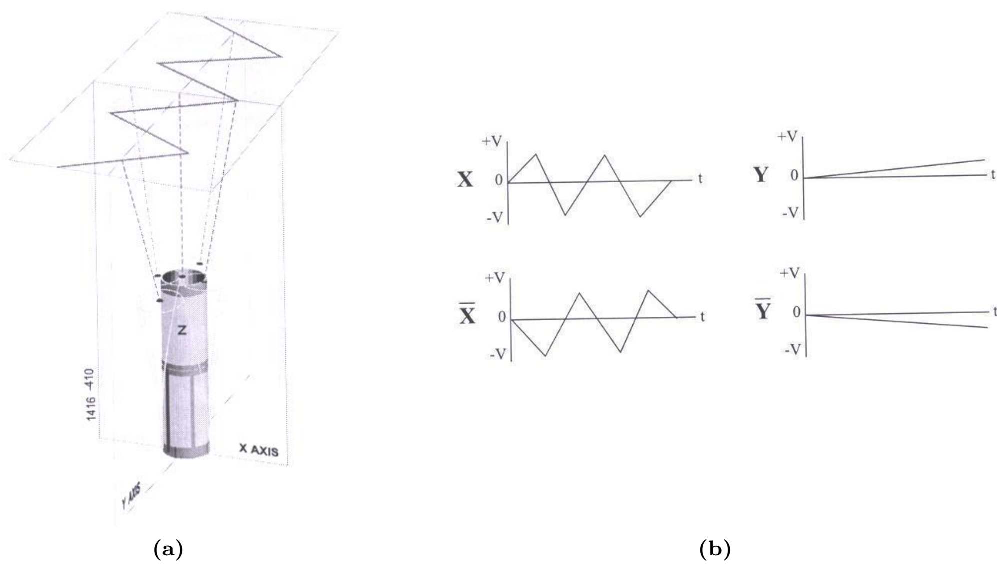

(a) **(b)**

Figure 2.13: The voltage characteristic when performing a raster scan with a piezoelectric tube scanner. The actual displacement of the tube, (a) and the applied signal to the different electrodes, (b). Images from [5].

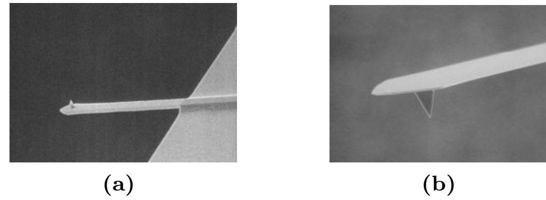

(a) (b)

Figure 2.14: Images, made with the scanning electron microscope (SEM), of a silicon cantilever (*a*) and tip (*b*) used for ICMAFM. Images from [5].

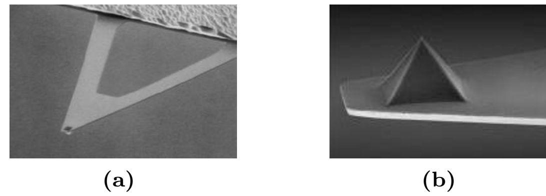

(a) (b)

Figure 2.15: SEM images of a silicon nitride (for CMAFM) cantilever (*a*) and tip (*b*). Images from [5].

differently to an applied voltage. This means that when increasing and decreasing the applied voltage linearly, the displacement of the piezoelectric element will be non-linear. When mapping a sample the trace and retrace images can therefore be shifted as result of the hysteresis effect.

2.2.3 AFM cantilevers and probes

The probe, attached to the cantilever, is the most crucial part of the atomic force microscope. As previously mentioned probes are generally made of silicon (Si), used for ICMAFM or silicon nitride (Si_3N_4), used for CMAFM. The fabrication and specifications of these probes therefore differ from each other and will be discussed in the following.

Silicon cantilevers primarily used for ICMAFM are generally rectangularly shaped (figure 2.14a). Important characteristics of cantilevers are the spring constant, resonant frequency, the cantilever configuration and the cantilever length. The ICMAFM cantilevers normally have a spring constant ranging from 2 to 200 N/m while the resonant frequency ranges from 200 to 400 kHz.

The rectangular shape is also called the single beam cantilever configuration and is about 125 μm in length [5]. The tip (figure 2.14b) and cantilever are produced by etching techniques. These tips have an end radius in the order of 5 to 10 nm. It is therefore possible to get high resolution images with these tips because how smaller the tips end radius is, the better it can detect sharp rises in the surface.

Contrary to the ICMAFM cantilevers, the CMAFM (silicon nitride) cantilevers have smaller spring constants, in the range of 0.10 N/m. This is accomplished by the V-shaped cantilever configuration and the fact that these cantilevers are longer, 100 to 200μm. The resonant frequency is lower than for ICMAFM and ranges from 10 to 30 kHz, depending on the length of the cantilever.

These specifications are used for soft CMAFM because this way, the force exerted on the surface is very small. Since the cantilever is not oscillating the relative low resonant frequency does not have any effect on the measurement. Often, there are multiple cantilevers, with different geometries, attached to a substrate. This way it is easy to switch cantilevers, which can be necessary when experimenting with different forces to map the surface. Also note the difference in tip shape between ICMAFM and CMAFM. The last one is more pyramid shaped and looks a bit blunt, while the ICMAFM tip is sharper.

Chapter 3

Scope of work

Within this chapter the methodology of the work done will be discussed. This not only includes describing, but also explaining why the specific procedure was followed. First the deposition of the films will be discussed followed by the analysis of the samples. Both parts are equally important in investigating the different parameters, and thus acquiring an insight in the sputtering process.

3.1 Thin film deposition

Investigating several important parameters, including the gas composition, the pressure and the formation of the bias voltage is the main goal of this project. Depositing the films in a controllable and reproducible way is crucial to the final result and since there are many adjustable parameters which influence the sputtering process, an accurate overview of all this is necessary.

3.1.1 The involved parameters

Several parameters can be adjusted, however not all the parameters are as important as another and therefore they will be discussed briefly. Not only the research parameters, but also the other important parameters kept constant will be discussed.

- *The gas which is used for sputtering.* As already discussed in the previous chapter the most common sputtering gas is argon. However it is also possible to mix some other gasses with this typical sputtering gas, which will result in variety of new conditions. To investigate the effect of mixing oxygen into the sputtering gas, a variety of samples will be made with different argon-oxygen relations.

- *Sputtering gas pressure.* Together with the sputtering current the pressure is one of the most important parameters because the pressure influences the mean free path (MFP) of the sputtered particles[1]. The MFP is the average distance which a particle travels before colliding with another particle. When the colliding particles have diameter d the effective

[1] Figures and equations from [14]

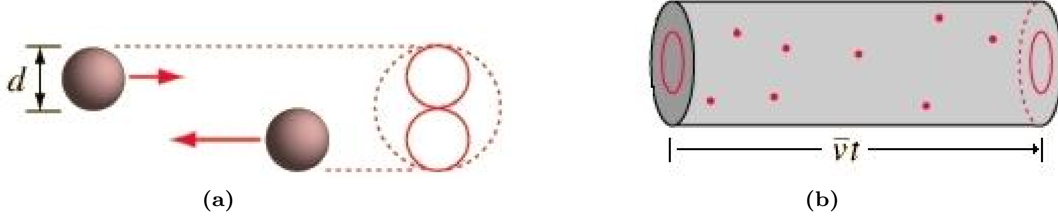

Figure 3.1: Two atoms colliding forming the collision cross-section (a) and the volume swept out by the cross-section in time t (b). Images from [14].

collision cross-section is defined as $A = \pi d^2$, as shown in figure 3.1a. This cross-section would sweep out volume $V = \pi d^2 \bar{v} t$ in time t (figure 3.1b). The total length of the path divided by the total amount of collisions gives the mean free path,

$$\lambda = \frac{\bar{v}t}{\pi d^2 \bar{v} t n_v} = \frac{1}{\pi d^2 n_v} \tag{3.1}$$

In this equation the assumption is made that the target particles are stationary by using the average molecular velocity, $\bar{v}$. Since the target atoms are moving around the average relative velocity should be used which can be calculated from the molecular speed distribution,

$$\bar{v}_{rel} = \sqrt{2}\bar{v} \tag{3.2}$$

The number of molecules per unit volume, n_v can be determined from the ideal gas law and Avogadro's number,

$$n_v = \frac{N_A P}{RT} \tag{3.3}$$

Also, the diameters of the colliding particles are equal in equation 3.1 which in the sputtering process is not a valid assumption. Therefore d^2 have to be replaced by $d_1 d_2$, where the indices 1 and 2 represent the diameters of the sputtered particles and the gaseous particles respectively. Now equation 3.2 and 3.3 can be substituted into equation 3.1 which results in,

$$\lambda = \frac{RT}{\sqrt{2}\pi d_1 d_2 N_A P} \tag{3.4}$$

With

λ	: the mean free path (MFP)	[m]
R	: the universal gas constant	[8,314 J·K^{-1}·mol^{-1}]
T	: the temperature of the gas	[K]
$d_{1,2}$	: the diameter of two colliding particles	[m]
N_A	: Avogadro's number	[$6.022 \cdot 10^{23}$ mol^{-1}]
P	: the pressure of the gas	[N·m^{-2}]

In other words the MFP is large when the pressure is low and/or the temperature is high, therefore the sputtered particles will collide only a few times when travelling from target to

substrate. The particles arriving at the substrate will have a relatively high kinetic energy which enhances the surface mobility. When the temperature is low and/or the pressure is high the MFP is relatively small which means that the sputtered particles will collide often before arriving at the substrate with lower kinetic energy. This will influence the growth of the thin film and therefore investigating this parameter is important.

- *The formation of the negative potential on the target.* As already explained in the previous chapter, the main difference between DC and RF sputtering is the formation of the bias voltage. This different method in formation of the negative potential could also affect the growth process which is why research towards this shall be done.

- *The sputtering current* is the amount of positively charged incident argon ions per second. The secondary electrons which are emitted at the target will mostly be trapped near the target, however some of them will also reach the anode. Therefore the sputtering current is a rough estimate for the amount of positively charged incident argon ions and also for the deposition rate of the film.

- *The sputtering time* influences the thickness of the grown film. When sputtering at a constant current the sputtered particles will arrive in a constant rate at the substrate. Therefore when measuring the thickness of a film grown with a long sputtering time the deposition rate can be calculated.

- *The substrate temperature* is parameter which has not been previously discussed, but nevertheless is a critical parameter. Due to the increased temperature the arriving atoms are left with a higher kinetic energy at the surface and thus are more mobile. This could effect the growth process in many ways. However this parameter will be kept constant at room temperature.

3.1.2 ATC-1800 deposition

The ATC-1800 is a magnetron sputtering system also capable of RF sputtering and is used for depositing the gold. To investigate the different parameters previously mentioned it is necessary to make several samples each with different sputter conditions. This way it is possible to investigate the influence of the pressure, argon-oxygen relation and hopefully also RF sputtering. The substrate used for the gold deposition is silicon (Si), which itself has a face-centered cubic (FCC) crystal structure. Although gold also has this same FCC crystal structure, it does not influence the growth of gold due to several reasons.

- The surface of the silicon used has a few nanometer thick native oxygen layer on it.

- Although the crystal structure matches, the sputtered gold particles are roughly 1.3 times larger than the silicon.

- Growing an adhesion layer before sputtering the gold film.

- Finally since sputtering is a process has a high deposition rate (∼10 nm/min for the ATC set-up used) and therefore the gold particles will not neatly arrange themselves when arriving at the substrate.

Therefore the gold is not deposited in a epitaxial growth mode but is instead grown in a polycrystalline form due to the crystal structure of the gold itself.

Creating an uniformly thin layer of gold is essential for this research. This is easily accomplished by just sputtering a ∼15 nm thick gold film onto the silicon substrate. However to improve the binding of the gold to the substrate an adhesion layer of molybdenum germanium (MoGe) is first sputtered and should be ∼1 nm in thickness. Also the silicon substrates should be cleaned before they are used for sputtering, which is done exactly the same each time. First the silicon substrate is rinsed with demi-water and blown dry with nitrogen (N_2). After mounting the substrate onto the substrate holder, it is rinsed with acetone and isopropanol (IPA) and then blown dry again with nitrogen. Then the substrate holder is placed into the ATC-1800 loadlock and in order to transfer the sample to the sputtering chamber, the loadlock is pumped down to below 10^{-6} mbar.

Table 3.1: MoGe adhesion sputter parameters: the pressure of the system, P, the gas flow rate (Ar and O_2), Φ, the sputtering current, I_s, the sputtering time, t_s and the rotation frequency, f_{rotat}.

	P (mTorr)	Φ_{Ar} (ml/min)	Φ_{O_2} (ml/min)	I_s (mA)	t_s (s)	f_{rotat} (Hz)
Pre-sputter	10	25	0	100	120	0.1
Sputter	10	25	0	100	45	0.1

All the sputtering, both adhesion and gold sputtering, has been done at room temperature. The adhesion layer is always grown with the same sputter parameters (table 3.1), which results in the same adhesion layer for the gold to grow on. The 45 seconds sputtering time will, with a MoGe deposition rate of 1.32 nm/min (at I_s = 100 mA), result in a ∼1 nm thick adhesion layer. No oxygen is used when sputtering the MoGe, because this would lead to oxidation of this layer. As shown in table 3.2, the sputter conditions for gold are the same as far as the rotation and

Table 3.2: Au sputter parameters.

	P (mTorr)	Φ_{Ar} (ml/min)	Φ_{O_2} (ml/min)	I_s (mA)	t_s (s)	f_{rotat} (Hz)
Pre-sputter	*	*	*	100	30	0.1
Sputter	*	*	*	100	90	0.1

sputtering current. However the pre- and sputtering time is different because gold has a higher deposition rate at these conditions (9.2 nm/min). Therefore, sputtering 90 seconds would result in a ∼15 nm thick film. The first three parameters (pressure, argon and oxygen flow) will be different for each sample. For each specific pressure (2, 5, 10 mTorr) six samples will be made, each with a different argon-oxygen relation ranging from 0% to 50% in steps of 10%. An extensive overview of the sputter parameters used for each sample can be found in appendix A.

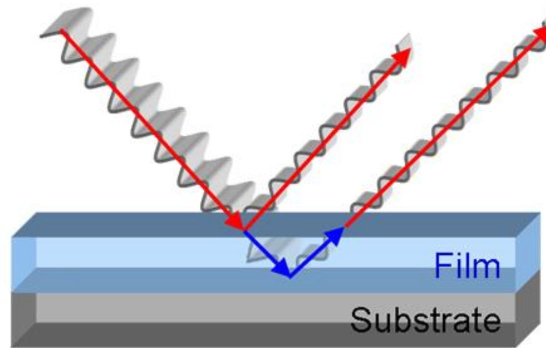

Figure 3.2: Simple representation of a x-ray measurement. The reflected x-rays are picked up by a detector and from the shift in position, the film thickness can be estimated. Image from [15].

3.1.3 Z-400 deposition

Although the ATC-1800 and the Z-400 sputtering systems use different sputtering techniques and most of the work is done with the ATC-1800, some samples created with the Z-400 might be necessary for comparison. The cleaning procedure is the same as when using the ATC-1800, however the sputtering procedure is different. Since only a few samples are needed for comparison the whole sputtering procedure of the Z-400 will not be discussed.

3.2 Analysis method

Different aspects of the grown films are important within this research project. As said before the roughness has a significant role in creating an understanding of the influence of different sputter parameters. However the sputter pressure and argon-oxygen relation could also influence the deposition rate and therefore the thickness of the grown films.

3.2.1 Film thickness

Thickness measurements were performed by x-ray reflectometry (XRR). A simple representation of this principle is given in figure 3.2. X-rays striking the surface of the film will be reflected off. The x-ray reflectivity can change due to the roughness and thickness of the film. XRR uses this effect by measuring the change in oscillation of the reflected x-rays as a function of the incident angle. Therefore XRR can provide information about the roughness, thickness and density of the grown film.

3.2.2 Film roughness

The roughness of the thin film surface is a crucial parameter and can be measured using different methods. Using x-ray reflectometry, not only the thickness but also information about the rough-

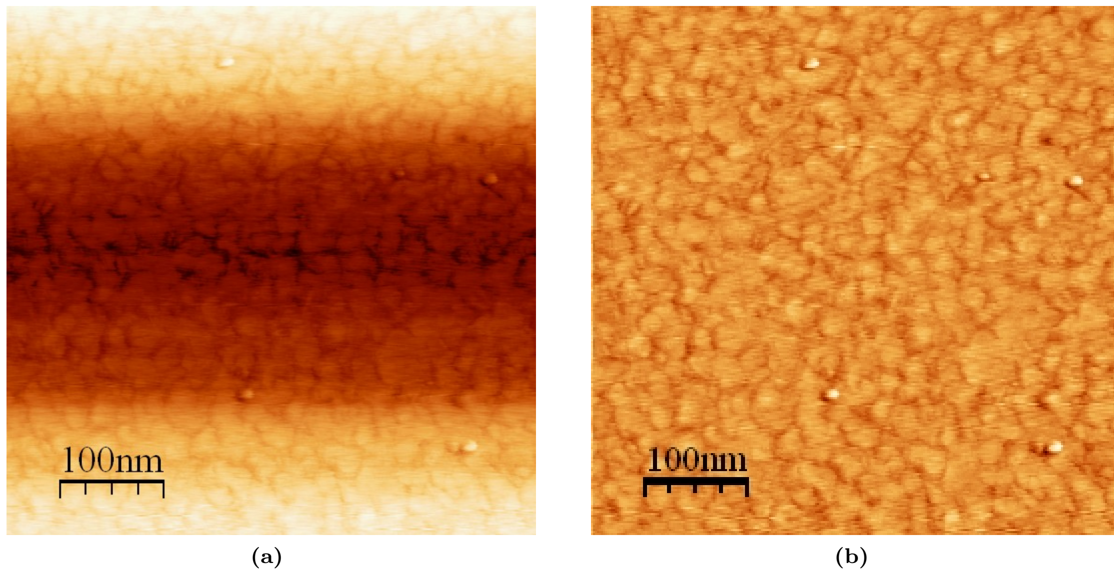

(a) (b)

Figure 3.3: Example of the same image with and without flatten filter applied. In (*a*) the raw topographic image is shown and in (*b*) the same image is presented only this time with flatten filter applied. Note the height differences between the two.

ness and density of the film can be obtained. There are also other methods to do this, and one of them is using AFM. The roughness of a surface can be defined in several ways. With x-ray reflectometry, the roughness is determined by the decrease in reflectivity. This is then computed in a single parameter which is calculated by the electronics of the machine. Instead of a single parameter as a result, AFM provides an actual image of the thin film surface. From this image, not only the roughness but many other analysis methods, such as 2D Fast Fourier Transformation (FFT) spectra, can be applied. This way, analysis is not limited by the standard methods, but also alternative methods can be used.

The theory of AFM is already discussed in chapter 2 and therefore this subject shall be discussed briefly. Both CMAFM and ICMAFM will be used for creating topographic images of the surface. Since the gold surface is quite soft and gold is also mobile at room temperature it is possible that when performing CMAFM the tip picks up a few gold atoms and drags them along, increasing the inaccuracy. With ICMAFM these effects are eliminated and possibly the images created are more accurate. An important parameter of ICMAFM is the resonance frequency of the cantilever used. Ranging from 70 to 300 kHz, the resonance frequency can act as a filter and thus influence the topographic image created.

The scanning probe microscope (SPM) used is the Veeco MultiMode SPM which provides many different imaging modes such as CMAFM, ICMAFM, STM. Different scanners can be used such as EV-type (10μm x 10μm) and J-type (125μm x 125μm) scanners. Nanoscope imaging software is used to drive the MultiMode SPM. For processing the topographic images WSxM is used [13]. The sample which is placed on the sample holder is never perfectly horizontal. Therefore the topographic image created can have height differences which are not due to the topography of the sample and thus need to be filtered away by using the flatten filter (figure 3.3.

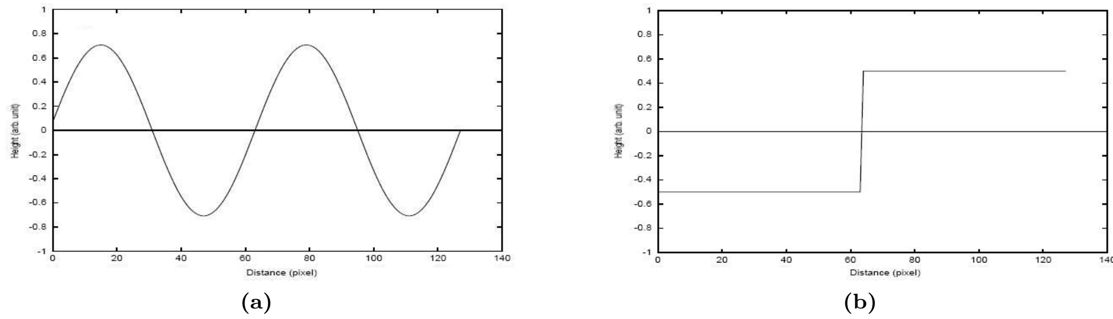

(a) (b)

Figure 3.4: Two different one-dimensional "surfaces" both zero mean and a total RMS value of 0.5. The sine function in (*a*) and the step function in (*b*). Images from [4].

3.2.3 Roughness analysis

The roughness of a surface can be determined and expressed in many different ways. The most commonly used parameter is the RMS roughness which is defined as,

$$RMS = \sqrt{\frac{1}{NM} \cdot \sum_{j=0}^{N} \sum_{i=0}^{M} z^2(x_i, y_j)} \tag{3.5}$$

With

RMS	: the root mean square roughness	[nm]
N	: the total amount of pixels in the x direction	[-]
M	: the total amount of pixels in the y direction	[-]
z	: the height value of each pixel	[nm]
x_i	: the pixel position in the x-direction	[-]
y_i	: the pixel position in the y-direction	[-]

With this RMS value the roughness of the entire surface can described. There are however some limiting conditions to this RMS roughness because it does not provide any information about the roughness related to any given lateral distance. This is also shown in figure 3.4, where there are two different one-dimensional "surfaces" displayed, figure 3.4a is a block function and figure 3.4b is sine function. The visual inspection suggests that the two surfaces have different RMS values, however they are exactly equal ($RMS = 0.5$). The RMS roughness is determined from the relative height variations in the topographic image and therefore depended on the height average z_0 (figure 3.4 z_0 was 0).

The RMS value then, can provide information about the roughness of a thin film surface, however it is not definitive. Therefore it might also be necessary to use other methods such as 2D FFT spectra.

Chapter 4

Results

The thickness and roughness of the created films are the most important parameters which have been investigated. Since x-ray and AFM measurements produce a lot of raw data, a selection of those results will be shown.

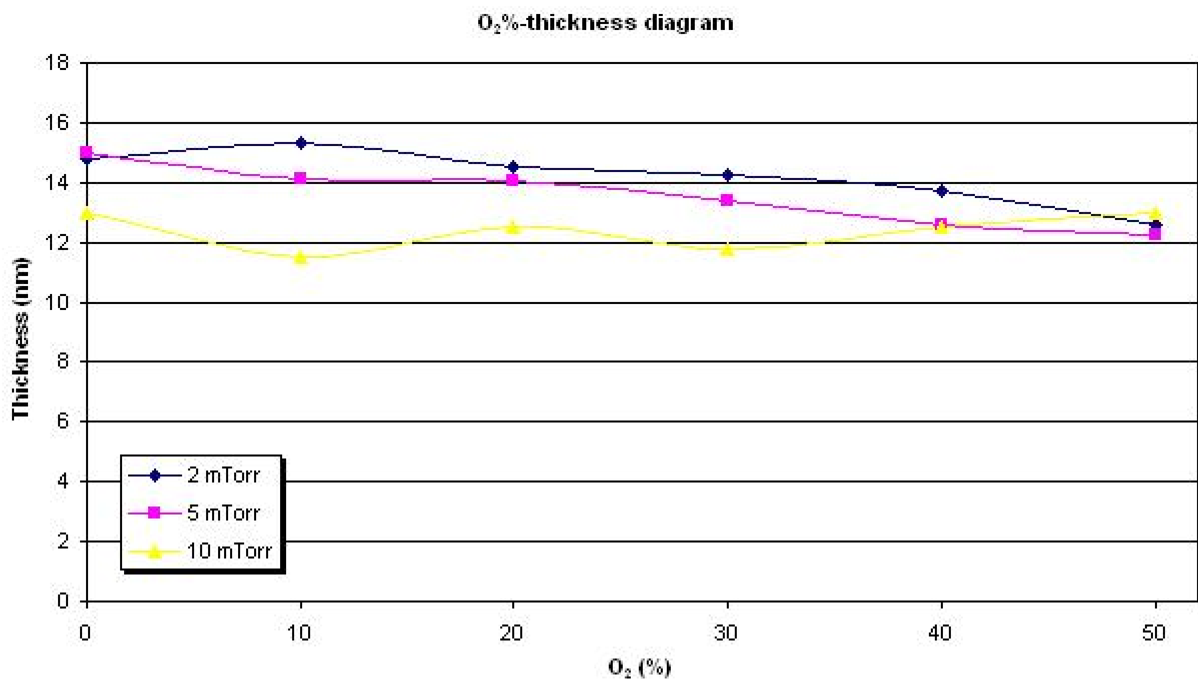

Figure 4.1: Thickness vs. O_2 percentage, measurements done by x-ray reflectometry.

4.1 Thickness of the films

4.1.1 XRR measurements

The results of the thickness measurements performed by x-ray reflectometry, are shown in figure 4.1. The three different sample series prove to show different film thicknesses. The inaccuracy in these thickness measurements are depended on the calibration and also on the wavelength of the x-rays (sub Angstrom). An accuracy of less than 0.1 nm is easily accomplished and therefore negligible.

For the lower pressures (2 and 5 mTorr) there is clearly a gradual decrease in thickness as the oxygen percentage increases. Increasing the oxygen concentration, also increases the amount of negative oxygen ions which bombard the anode. One might expect the negative ions would sputter away a large amount of deposited material, however due to the large anode area the effect at the substrate is relatively small. Also, oxygen is roughly two times lighter than argon and therefore is not as effective in sputtering. Nevertheless, some of the deposited gold is sputtered from the substrate and this effect still increases together with the oxygen concentration. The ascent of both 2 and 5 mTorr is the same, however in absolute thickness 5 mTorr is, apart from 0% and 50% oxygen, 0.5 to 1 nm thinner than 2 mTorr.

At higher pressure (10 mTorr) the thickness decreases even more and interestingly, 10 mTorr does not show the same ascent as the lower pressures, but has roughly the same thickness throughout the whole range. This is probably caused due to the fact that at higher pressure, the sputtered gold particles collide more often when travelling from target to substrate. This results in a more diffusive way of travelling from target to substrate and therefore less gold particles actually reach the substrate. Thus the deposition rate goes down a little and since the sputtering time is kept constant, the deposited film is up to 3 nm thinner. The lack of this ascent at higher pressure can also be explained by the collision probability. Not only the sputtered gold particles are colliding more often, also the oxygen ions are. Together with the weight difference between argon and oxygen, it is probable that the oxygen ions arriving at the substrate simply do not have enough energy to sputter many gold atoms. The difference in film thicknesses throughout the whole 10 mTorr range can be partially attributed by the inaccuracy in sputtering time. An inaccuracy of ± 3 seconds sputtering time would result in a ± 0.5 nm thinner or thicker film.

4.2 Roughness of the films

4.2.1 First AFM set-up

The sample roughness has been determined using different AFM modes. CMAFM was the first choice for imaging, regardless the high surface mobility which gold has at room temperature and the possible lateral forces such as drag. CMAFM was performed using a Veeco MultiMode SPM piezoelectric scanner in combination with RHK electronics (SPM 1000, AIM-DI and VScan) and relative old Nanoscope software (which is also developed by Veeco Instruments). With each scan

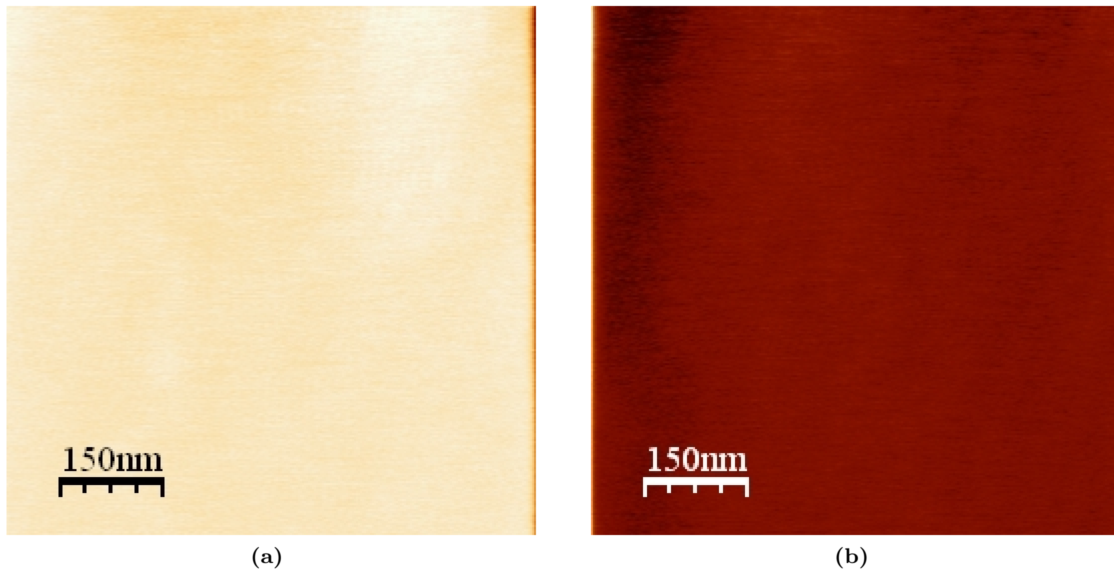

(a) (b)

Figure 4.2: Trace (a) and retrace (b) images of CMAFM on a Z-400 sample. Note the step-like feature at right side in (a) and left side in (b).

two topographic images are created (trace and retrace). When trace and retrace scans show the same features it indicates that the sample surface is being imaged. An image is composed of X, Y and Z data where the Z component is displayed as colour differences. Typically the Z scale is from 0 to 10 nm, where 0 nm is black and 10 nm is white. The inaccuracy in AFM measurements is in principle very small since it is possible to measure steps of atomic variations. Inaccuracy in RMS value however is for instance strongly depended on the amount of noise. There is, however no systematical inaccuracy and therefore it will not be taken into account, however RMS inaccuracy will be discussed later on.

From the start there were quite some problems with this AFM set-up and in figure 4.2 one of the first results is shown, made from a test sample deposited in the Z-400. The tip makes trace and retrace scans of the surface, thus one image is composed only from scan lines in for example the x-direction and the other image is then composed only from scan lines in the $-x$-direction. These images each show some step-like feature at the start of each line which is probably caused by the tip. When the tip changes direction (i.e. from x to $-x$) it is possible that the tip tilts and deforms the gold surface (this because gold is quite soft at room temperature). These step-like features have an average height of 6 nm and therefore decrease the resolution of the rest of the image enormously.

This tilting of the tip when changing directions has a direct relation to the force the tip exerts on the sample and can be adjusted on the piezoelectric scanner. A voltage is set that, depending on the spring constant of the cantilever used, determines the force. Finally an optimum was found for the exerted force which resulted in scans without these step-like features (figure 4.3). The upper two images are 500x500 nm scans and the lower two 750x750 nm scans, both of the same sample. Therefore it should be possible to recognise some of features of the 500x500 nm scan in the

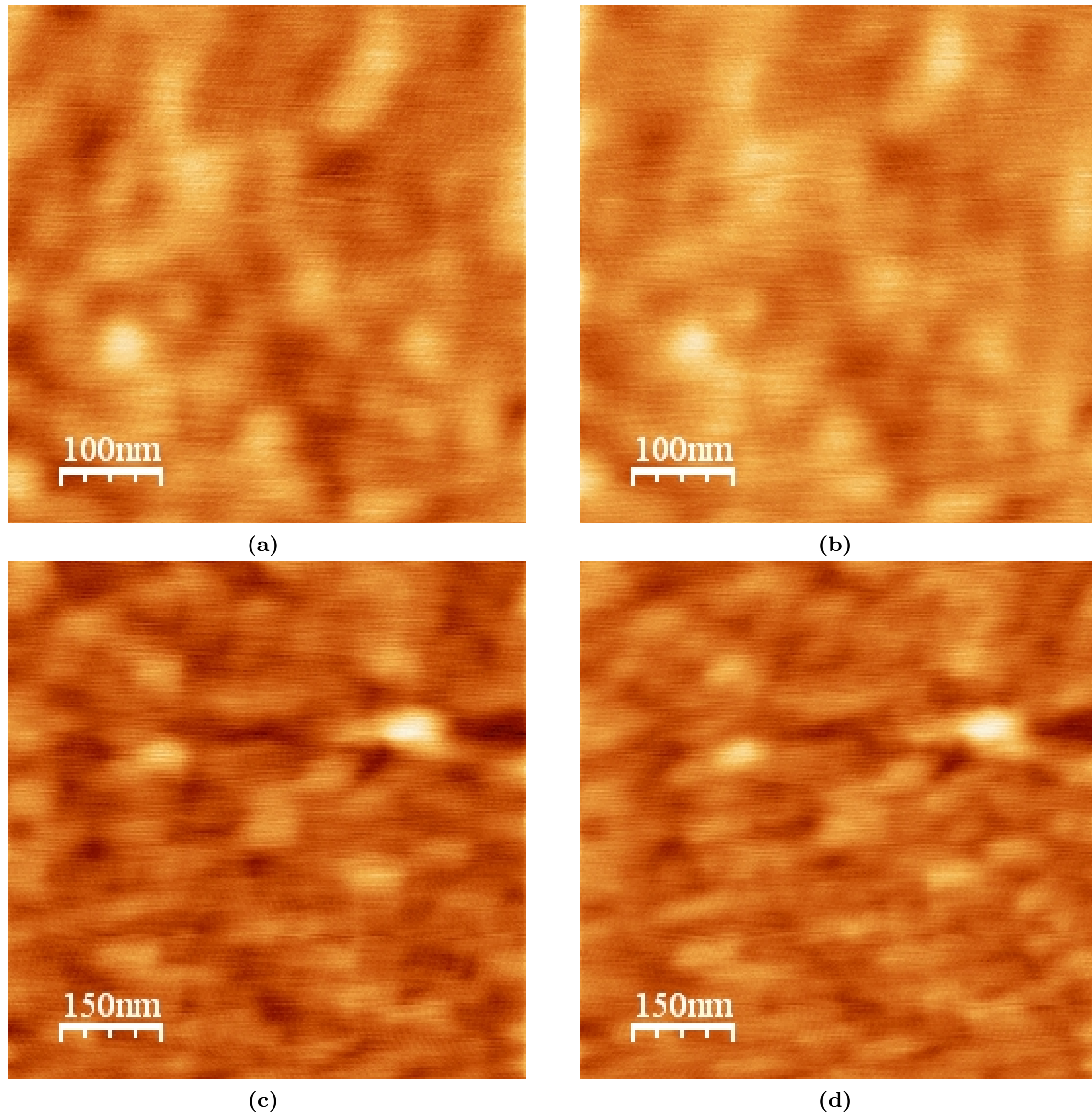

(a) (b) (c) (d)

Figure 4.3: Final results of the first AFM set-up using CMAFM. The first two images (trace, (*a*) and retrace, (*b*)) are 500x500 nm scans of the same sample used in figure 4.2. 750x750 nm scans are shown in (*c*) and (*d*), also from the same sample. Expected was that the features in (*a*) and (*b*) would be retraceable in (*c*) and (*d*), however due to piezoelectric drift this is not entirely visible.

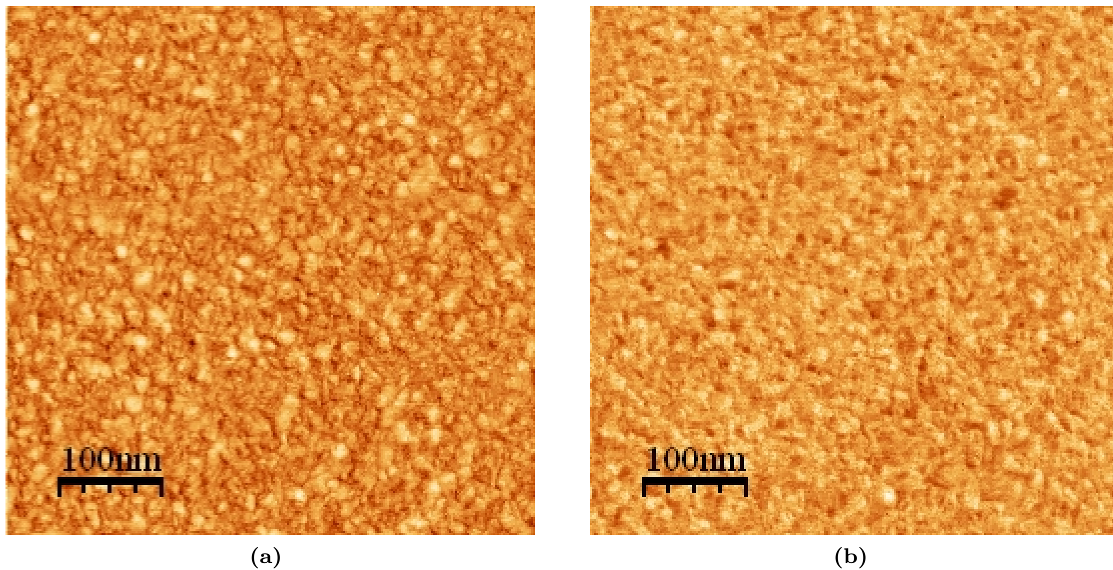

(a) (b)

Figure 4.4: First CMAFM topographic images, made with the second AFM set-up. Trace and retrace images match indicating that the sample surface has been scanned. Also the images appear less noisy and therefore are more accurate.

larger scan. Due to piezoelectric drift in the slow scan axis (y-direction) this is not immediately visible, however when looking closely there are some similarities between them. Piezoelectric drift is constant in one direction and eventually it goes away while scanning. When scanning against the drift the resulting image look compressed and when scanning with the drift the image seems to be stretched. Sometimes it can also be convenient to scan perpendicular to the drift direction resulting in scans with the same amount of drift in the same direction.

With this AFM set-up there were some problems in the beginning and although those were resolved the results were not as promising as hoped. First of all it was very hard and took quite some time to get the AFM working properly and secondly the resulting images were noisy and streaky (figure 4.3). Therefore a second AFM set-up was used to look wether improvements could be made just by using a different set-up.

4.2.2 Second AFM set-up

The piezoelectric scanner used is the same as in the previous AFM set-up, namely the Veeco MultiMode SPM. However the electronics together with the new software are different in this set-up and both have been developed by Veeco Instruments. Again CMAFM was the first mode in which the samples were scanned and from the start it went a lot better than with the previous set-up. As shown in figure 4.4 the images show no drift as the grains are not deformed in trace and retrace scans. Also the two images match though there is some overall height difference and the two images show not so much noise as in de previous results. Another set of CMAFM images are shown in figure 4.5. The raw topographic data is shown in the first two images where some high frequent tip oscillations are also visible. It is certain that these oscillations are not part of the

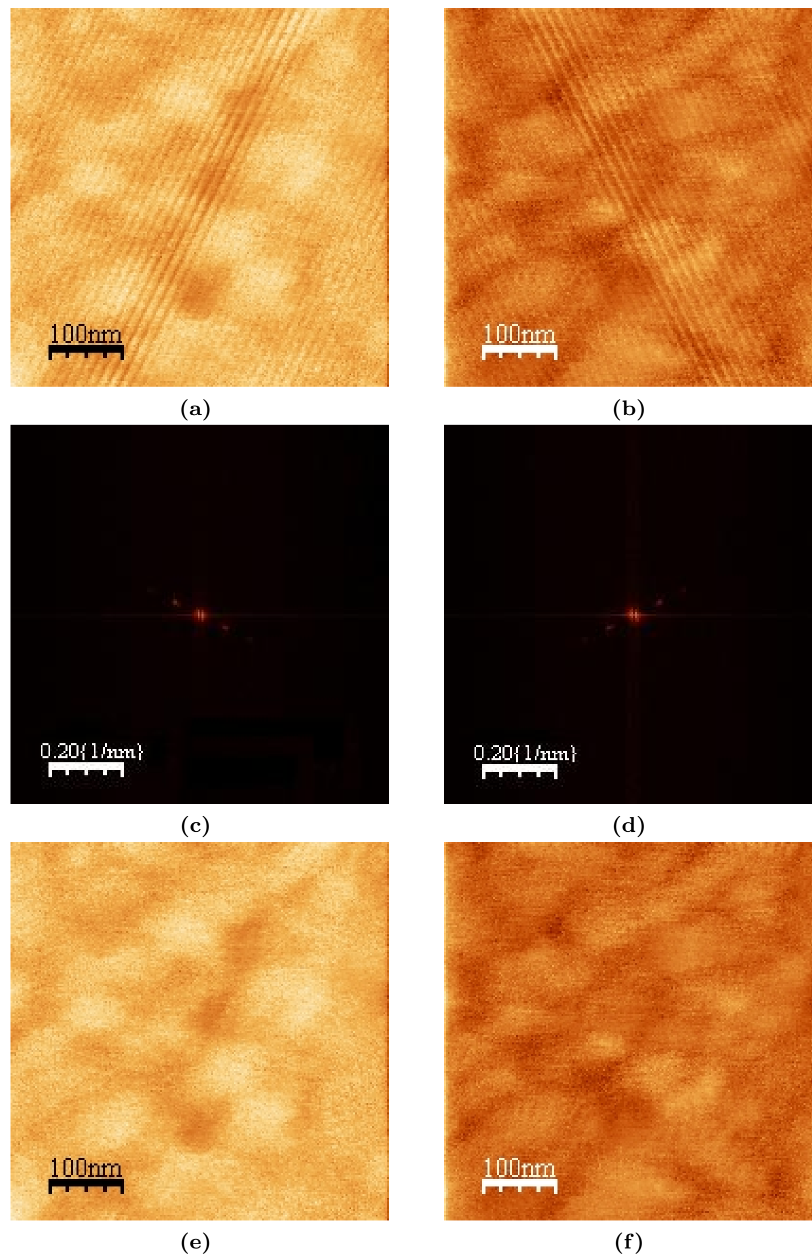

Figure 4.5: Images with tip oscillations due to high gains, the 2D FFT spectra and the resulting images after filtering away the oscillations. In (*a*) and (*b*) the trace and retrace topographic images are shown with tip oscillations. These oscillations can also be visualized by making a 2D FFT spectra as shown in (*c*) and (*d*). The cluster in the centre of the image is the actual data and the two bright spots not far from it indicate high frequent data (the oscillations). These spots can be filtered away resulting in the same image as in (*a*) and (*b*) only now without the oscillations: (*e*) and (*f*).

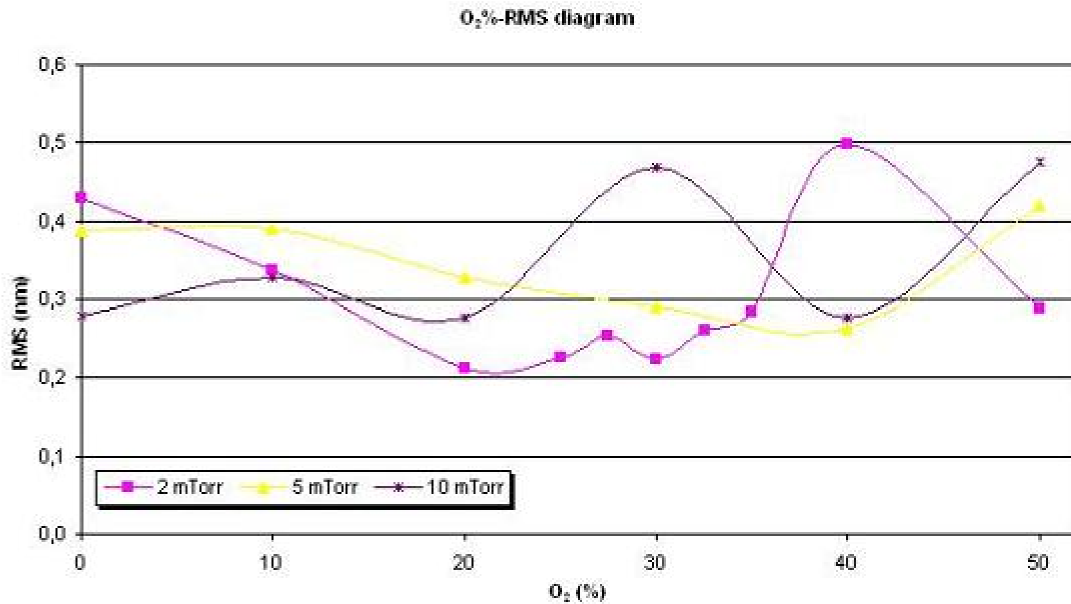

Figure 4.6: RMS Roughness vs. O_2 percentage, measurements done by AFM and RMS value is calculated with WSxM.

actual topography because the direction of the oscillations differ in trace and retrace scans. Luckily these oscillations are also visible in a 2D FFT spectra shown in the second pair of images. The data from the first to images is now converted into a frequency spectra. In the centre the low frequent topographic data is displayed and because the oscillations are high frequent, the oscillation data will be more off centre as also shown in the two images. In the 2D FFT spectra, these two spots can be filtered away resulting in two topographic images without the oscillations (last pair). These filtering techniques are applied when necessary to improve the accuracy of the results.

Using this AFM set-up proved to be easier and also quite a bit faster therefore all the different samples were imaged using CMAFM. This led to a vast amount of topographic images, all which had to be analysed. This is done not by inspecting each image, but by using the RMS roughness, which is explained in the previous chapter. Although the RMS value is not a very conclusive parameter, hopefully it could give an indication about the dependence of the roughness as function of pressure and argon-oxygen relation.

In figure 4.6 the RMS roughness is given as function of the oxygen percentage at different pressures. The 2 mTorr samples (which were the first to be made and measured) showed an descent from 0 to 30% and than a sharp increase in roughness at 40%. Four extra samples were made and measured to check wether this progress also fitted with other argon-oxygen relations (75/25, 72.5/27.5, 67.5/32.5, 65/35) and as shown in figure 4.6. The samples and RMS roughness seem to fit in nicely. The 5 mTorr showed some similarities with the 2 mTorr although it looks like the curve is shifted to the right (especially the minimum). The sharp increase which 2 mTorr has at 40%, is probably also shifted only now disappeared in the 5 mTorr curve. This trend however does not persist at a higher pressure (10 mTorr), instead the difference in RMS values increases

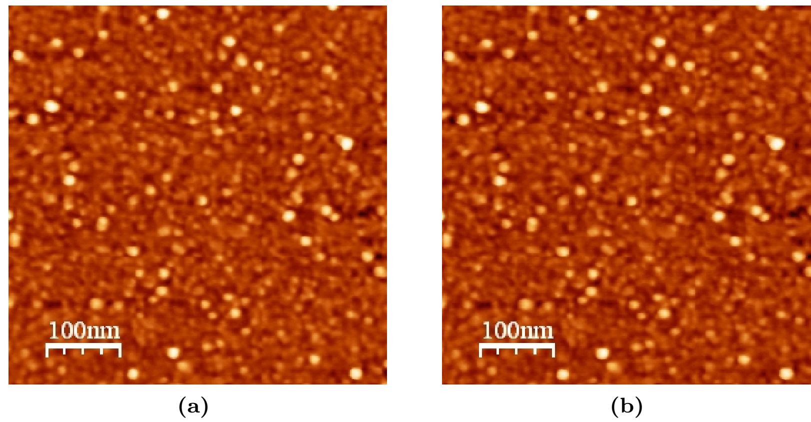

Figure 4.7: First results of the topographic images created with ICMAFM.

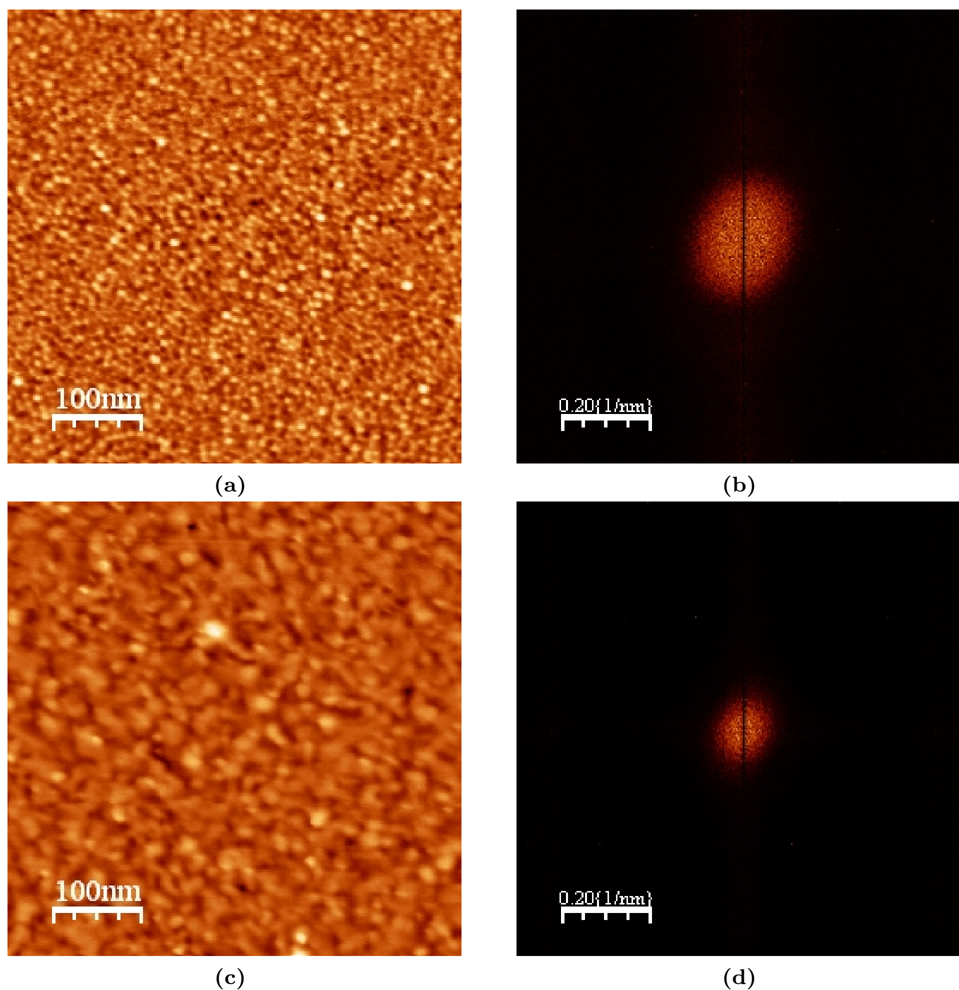

Figure 4.8: Example of how grain size is also retraceable in the 2D FFT plot. In (*a*) the grains are very small and therefore also high frequent as is also visible in (*b*). The second image in (*c*) has larger grains which is also visible in the FFT plot (*d*). When then comparing (*b*) and (*d*) with each other it is clearly visible that (*b*) has smaller grains which are therefore high frequent.

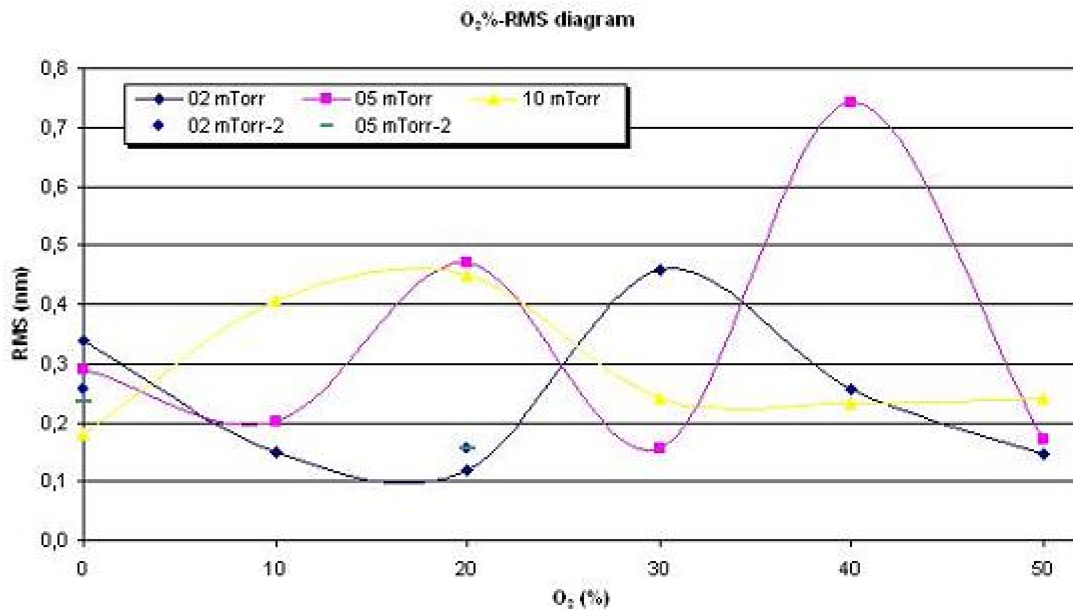

Figure 4.9: RMS roughness vs. O_2 percentage, measurements done by ICMAFM on the second AFM set-up while keeping the parameters which could influence the measurement constant.

throughout the whole range. Although these results looks quite promising the topographic images still were quite noisy which affects the inaccuracy a great deal. Therefore also ICMAFM was also performed on the same samples.

First the 10 mTorr samples were measured with ICMAFM improving the quality of the images enormously as shown in figure 4.7. The two images (trace and retrace) again match indicating that the actual surface has been scanned. With ICMAFM no filters apart from the flatten filter were needed. Figure 4.4 (CMAFM) showed a lot of distortion increasing the inaccuracy, whereas figure 4.7 has very little distortion. Also, in the contrary to CMAFM, ICMAFM enables a fast scanning rate and also easy adjustment. As already explained before a 2D FFT plot show the same topographic data in a frequency domain and with the noise gone the 2D FFT plot can now also provide information about the grains size as shown in figure 4.8. Next to the two topographic images, also 2D FFT images with the same topographic data are displayed. The topographic images are both 500x500 nm scans from different samples. Figure 4.8a has more grains in the same area as figure 4.8c which indicates that the grains in figure 4.8a are high frequent, what also can be derived from the 2D FFT images.

Due to the improvement made with ICMAFM, all the samples were again measured in order to get more accurate overview. To decrease inaccuracy everything was kept constant while measuring including the tip used, the calibration and so on. This is necessary because AFM has a huge amount of parameters that can influence the measurements. Again ICMAFM proved to be the better imaging mode with similar results as previously shown.

In figure 4.9 the final graph is displayed which shows different curves for each pressure. The four extra measurements (02 mTorr-2 and 10 mTorr-2) were added to check how much difference

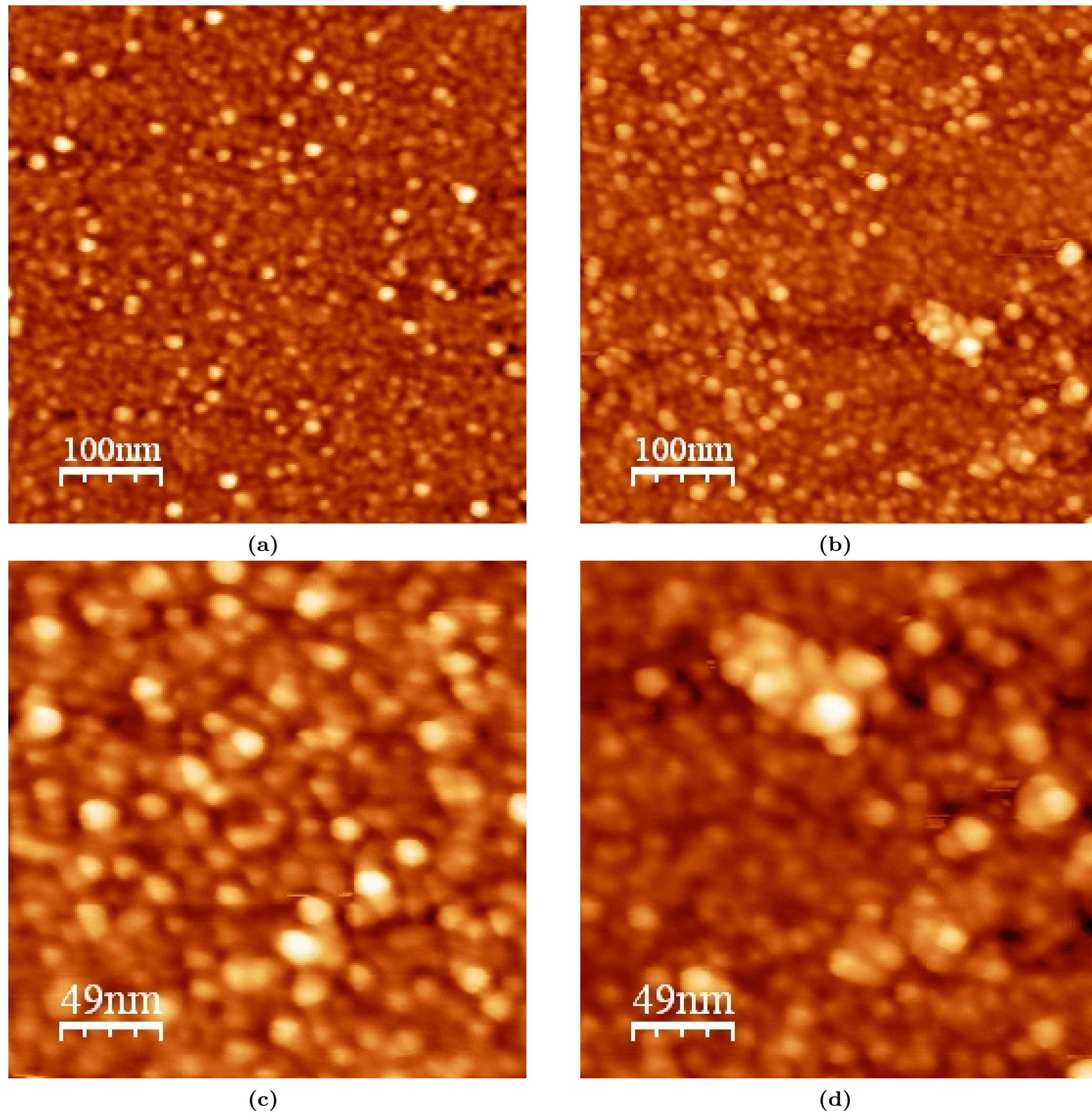

(a) **(b)** **(c)** **(d)**

Figure 4.10: AFM images showing the RMS roughness complications. Two different samples are shown here with different RMS roughness values which is mainly due to the large cluster on the second image, (*b*). Image (*a*) has a RMS roughness value of 0.65 nm whereas the second image (*b*), has an RMS roughness value of 1.0 nm. The other two images are zoom from (*b*), (*c*) is a zoom from the upper left corner and (*d*) from the lower right corner, both with dimensions of ∼250x250 nm.

there was in roughness between old and new samples. None of the new and old samples really have the same RMS value, which is probably also due to the inaccuracy in the RMS roughness which will be discussed later but also due to the age of the sample. Energetically speaking a flat surface is not the favourite condition for a material to be in, it would rather be in bulk form. Therefore, when a sample get older, the surface (especially from gold since gold is very mobile at room temperature) could start to crystallize and form larger grains which then again results in an increase in RMS roughness.

The ICMAFM results do not show any agreement with the previous CMAFM results (figure 4.6) apart from the order of magnitude. This could be an indication of the inaccuracy of CMAFM measurements however it may also be due to the calibration and settings used for either CMAFM of ICMAFM. Also, the second peak in the 5 mTorr curve is not really expected because the RMS roughness is two times as large than the other measurements.

The RMS roughness is, as already explained before, not a very definitive indication of the actual surface topography and roughness. This was also found during measurements which will be explained using figure 4.10. In total four images are shown, the upper two are from two different samples and have RMS roughness values of 0.65 and 1.0 nm respectively. This difference is mainly caused by the grain cluster in figure 4.10b although the rest of the image has also more height variation which also contributes to an increased RMS value. The lower two images are magnifications of figure 4.10b, where figure 4.10c is made from the upper left corner ($RMS = 0.92$ nm) and 4.10d from the lower right corner ($RMS = 1.2$ nm). The increased roughness due to this cluster does not have to be a representative indication for the rest of the surface. RMS roughness therefore has a large inaccuracy and is possible not the best analysis method.

Chapter 5

Conclusions & Recommendations

5.1 Conclusions

Different aspects of sputtered gold films have been investigated and from the results several conclusions can be drawn. Some might not be the conclusions looked for, but can provide an insight which is important for further research.

- Adding oxygen to the sputtering gas at low pressure (2 & 5 mTorr), results in sputtering the substrate and therefore in thinner films. This effect increases together with the oxygen concentration. At high sputtering pressure (10 mTorr) the deposition goes down and adding oxygen is not so effective any more, both can be explained by the increased collision probability at this higher pressure.

- Caution should be preserved when imaging gold samples with SPM. When using CMAFM the gold surface is easily deformed by tip tilting, due to gold softness and high mobility at room temperature. Therefore CMAFM might not be the best imaging mode to use. ICMAFM can provide the alternative, because ICMAFM is also used for biological systems (which are often soft). In comparison to the CMAFM results, ICMAFM did improve the accuracy of the results enormously.

- The analysis of the data is the most crucial part of the research project. Unfortunately, the RMS roughness did not prove to be an accurate parameter for the surface roughness. This is caused by the lateral dependence and also due to the fact that two differently formed surfaces can give the same RMS value. 2D FTT spectra could give an indiction of grain size and distribution, however not on actual roughness.

- It is still not very clear how the sample age influences the sample roughness. This can be partially attributed to the RMS roughness but it was also not the main goal of the project and therefore not fully investigated.

- Unfortunately investigating the effect of radio frequency sputtering was not completed due

to lack of time. Also the comparison with the Z-400 was not completed, because the analysis did not go very well.

5.2 Recommendations

For further research towards the roughness of sputtered gold films several improvements can be made which are also listed.

- For a better insight of the processes which occur when sputtering with oxygen it could prove to be very useful to also investigate RF sputtering because it could provide more information about the different aspects of reactive sputtering with oxygen.
- Although ICMAFM seems to give accurate results, there are still some things which can be improved. By scanning the same sample surface multiple times (5 to 10 times) on different areas a more accurate overview of the surface can be created. This also improves the accuracy of the analysis applied to the data.
- As far as the roughness analysis is concerned, a whole different method is required. RMS roughness analysis simply fails to provide any reliable information. The definition of roughness can be broadly interpret and therefore this should also be taken into account looking for another method. Using WSxM as processing software enables the possibility to save the data in an ACSII matrix which than can be loaded in other mathematical software such as Mathlab. This way, developing a new roughness analysis technique is relatively easy.

Appendix A

Au-film process parameters

All samples have been made with a MoGe adhesion layer which was sputtered under the same deposition conditions every time (table A.1).

Table A.1: MoGe deposition conditions

	P (mTorr)	Φ_{Ar} (ml/min)	Φ_{O_2} (ml/min)	I_s (mA)	t_s (s)	f_{rotat} (Hz)
Pre-sputter	10	25	0	100	120	0.1
Sputter	10	25	0	100	45	0.1

A.1 02 mTorr samples

22-02 02mT (100.0)

	Pre-sputter	Sputter
P (mTorr)	02	02
Φ_{Ar} (ml/min)	25	25
Φ_{O_2} (ml/min)	0	0
f_{rotat} (Hz)	0.1	0.1
t_s (s)	30	90
I_s (mA)	100	100
U_{MoGe} (V)	304	311
U_{Au} (V)	470	466

Fabrication date: 22-02-2007

CMAFM date: 26-02-2007

ICMAFM date: 12-04-2007

22-2 02mT (90.10)

	Pre-sputter	Sputter
P (mTorr)	02	02
Φ_{Ar} (ml/min)	25	25
Φ_{O_2} (ml/min)	2.8	2.8
f_{rotat} (Hz)	0.1	0.1
t_s (s)	30	90
I_s (mA)	100	100
U_{MoGe} (V)	305	306
U_{Au} (V)	487	487

Fabrication date: 22-02-2007

CMAFM date: 26-02-2007

ICMAFM date: 12-04-2007

02-03 02mT (80.20)

	Pre-sputter	Sputter
P (mTorr)	02	02
Φ_{Ar} (ml/min)	25	25
Φ_{O_2} (ml/min)	6.3	6.3
f_{rotat} (Hz)	0.1	0.1
t_s (s)	30	90
I_s (mA)	100	100
U_{MoGe} (V)	300	300
U_{Au} (V)	500	500

Fabrication date: 02-03-2007

CMAFM date: 02-03-2007

ICMAFM date: 12-04-2007

03-03 02mT (75.25)

	Pre-sputter	Sputter
P (mTorr)	02	02
Φ_{Ar} (ml/min)	25	25
Φ_{O_2} (ml/min)	8.3	8.3
f_{rotat} (Hz)	0.1	0.1
t_s (s)	30	90
I_s (mA)	100	100
U_{MoGe} (V)	300	308
U_{Au} (V)	507	510

Fabrication date: 03-03-2007

CMAFM date: 03-03-2007

ICMAFM date: -

02-03 02mT (72,5.27,5)

	Pre-sputter	Sputter
P (mTorr)	02	02
Φ_{Ar} (ml/min)	25	25
Φ_{O_2} (ml/min)	9.5	9.5
f_{rotat} (Hz)	0.1	0.1
t_s (s)	30	90
I_s (mA)	100	100
U_{MoGe} (V)	297	309
U_{Au} (V)	513	516

Fabrication date: 03-03-2007

CMAFM date: 03-03-2007

ICMAFM date: -

02-03 02mT (70.30)

	Pre-sputter	Sputter
P (mTorr)	02	02
Φ_{Ar} (ml/min)	25	25
Φ_{O_2} (ml/min)	10.7	10.7
f_{rotat} (Hz)	0.1	0.1
t_s (s)	30	90
I_s (mA)	100	100
U_{MoGe} (V)	298	309
U_{Au} (V)	517	519

Fabrication date: 02-03-2007

CMAFM date: 02-03-2007

ICMAFM date: 12-04-2007

03-03 02mT (67,5.32,5)

	Pre-sputter	Sputter
P (mTorr)	02	02
Φ_{Ar} (ml/min)	25	25
Φ_{O_2} (ml/min)	12.0	12.0
f_{rotat} (Hz)	0.1	0.1
t_s (s)	30	90
I_s (mA)	100	100
U_{MoGe} (V)	300	310
U_{Au} (V)	520	521

Fabrication date: 03-03-2007

CMAFM date: 03-03-2007

ICMAFM date: -

03-03 02mT (65.35)

	Pre-sputter	Sputter
P (mTorr)	02	02
Φ_{Ar} (ml/min)	25	25
Φ_{O_2} (ml/min)	13.5	13.5
f_{rotat} (Hz)	0.1	0.1
t_s (s)	30	90
I_s (mA)	100	100
U_{MoGe} (V)	295	310
U_{Au} (V)	524	525

Fabrication date: 03-03-2007

CMAFM date: 03-03-2007

ICMAFM date: -

02-03 02mT (60.40)

	Pre-sputter	Sputter
P (mTorr)	02	02
Φ_{Ar} (ml/min)	25	25
Φ_{O_2} (ml/min)	16.7	16.7
f_{rotat} (Hz)	0.1	0.1
t_s (s)	30	90
I_s (mA)	100	100
U_{MoGe} (V)	300	301
U_{Au} (V)	530	533

Fabrication date: 02-03-2007

CMAFM date: 02-03-2007

ICMAFM date: 12-04-2007

02-03 02mT (50.50)

	Pre-sputter	Sputter
P (mTorr)	02	02
Φ_{Ar} (ml/min)	20	20
Φ_{O_2} (ml/min)	20	20
f_{rotat} (Hz)	0.1	0.1
t_s (s)	30	90
I_s (mA)	100	100
U_{MoGe} (V)	300	302
U_{Au} (V)	547	550

Fabrication date: 02-03-2007

CMAFM date: 02-03-2007

ICMAFM date: 12-04-2007

A.2 02 mTorr 13-04 samples

13-04 02mT (100.0)

	Pre-sputter	Sputter
P (mTorr)	02	02
Φ_{Ar} (ml/min)	25	25
Φ_{O_2} (ml/min)	0	0
f_{rotat} (Hz)	0.1	0.1
t_s (s)	30	90
I_s (mA)	100	100
U_{MoGe} (V)	302	309
U_{Au} (V)	469	470

Fabrication date: 13-04-2007

CMAFM date: -

ICMAFM date: 13-04-2007

13-04 02mT (80.20)

	Pre-sputter	Sputter
P (mTorr)	02	02
Φ_{O_2} (ml/min)	6.3	6.3
f_{rotat} (Hz)	0.1	0.1
t_s (s)	30	90
I_s (mA)	100	100
U_{MoGe} (V)	301	305
U_{Au} (V)	499	501

Fabrication date: 13-04-2007

CMAFM date: -

ICMAFM date: 13-04-2007

A.3 05 mTorr samples

06-03 05mT (100.0)

	Pre-sputter	Sputter
P (mTorr)	05	05
Φ_{Ar} (ml/min)	25	25
Φ_{O_2} (ml/min)	0	0
f_{rotat} (Hz)	0.1	0.1
t_s (s)	30	90
I_s (mA)	100	100
U_{MoGe} (V)	298	309
U_{Au} (V)	450	449

Fabrication date: 06-03-2007

CMAFM date: 06-03-2007

ICMAFM date: 12-04-2007

06-03 05mT (90.10)

	Pre-sputter	Sputter
P (mTorr)	05	05
Φ_{Ar} (ml/min)	25	25
Φ_{O_2} (ml/min)	2.8	2.8
f_{rotat} (Hz)	0.1	0.1
t_s (s)	30	90
I_s (mA)	100	100
U_{MoGe} (V)	298	309
U_{Au} (V)	475	477

Fabrication date: 06-03-2007

CMAFM date: 06-03-2007

ICMAFM date: 12-04-2007

06-03 05mT (80.20)

	Pre-sputter	Sputter
P (mTorr)	05	05
Φ_{Ar} (ml/min)	25	25
Φ_{O_2} (ml/min)	6.3	6.3
f_{rotat} (Hz)	0.1	0.1
t_s (s)	30	90
I_s (mA)	100	100
U_{MoGe} (V)	301	310
U_{Au} (V)	497	497

Fabrication date: 06-03-2007

CMAFM date: 06-03-2007

ICMAFM date: 12-04-2007

06-03 05mT (70.30)

	Pre-sputter	Sputter
P (mTorr)	05	05
Φ_{Ar} (ml/min)	25	25
Φ_{O_2} (ml/min)	10.7	10.7
f_{rotat} (Hz)	0.1	0.1
t_s (s)	30	90
I_s (mA)	100	100
U_{MoGe} (V)	297	309
U_{Au} (V)	515	517

Fabrication date: 06-03-2007

CMAFM date: 06-03-2007

ICMAFM date: 12-04-2007

07-03 05mT (60.40)

	Pre-sputter	Sputter
P (mTorr)	05	05
Φ_{Ar} (ml/min)	25	25
Φ_{O_2} (ml/min)	16.7	16.7
f_{rotat} (Hz)	0.1	0.1
t_s (s)	30	90
I_s (mA)	100	100
U_{MoGe} (V)	300	309
U_{Au} (V)	532	533

Fabrication date: 07-03-2007

CMAFM date: 07-03-2007

ICMAFM date: 12-04-2007

07-03 05mT (50.50)

	Pre-sputter	Sputter
P (mTorr)	05	05
Φ_{Ar} (ml/min)	20	20
Φ_{O_2} (ml/min)	20	20
f_{rotat} (Hz)	0.1	0.1
t_s (s)	30	90
I_s (mA)	100	100
U_{MoGe} (V)	300	309
U_{Au} (V)	546	547

Fabrication date: 07-03-2007

CMAFM date: 07-03-2007

ICMAFM date: 12-04-2007

A.4 05 mTorr 13-04 samples

13-04 05mT (100.0)

	Pre-sputter	Sputter
P (mTorr)	05	05
Φ_{Ar} (ml/min)	25	25
Φ_{O_2} (ml/min)	0	0
f_{rotat} (Hz)	0.1	0.1
t_s (s)	30	90
I_s (mA)	100	100
U_{MoGe} (V)	302	309
U_{Au} (V)	449	451

Fabrication date: 13-04-2007

CMAFM date: -

ICMAFM date: 13-04-2007

13-04 05mT (80.20)

	Pre-sputter	Sputter
P (mTorr)	05	05
Φ_{O_2} (ml/min)	6.3	6.3
f_{rotat} (Hz)	0.1	0.1
t_s (s)	30	90
I_s (mA)	100	100
U_{MoGe} (V)	299	302
U_{Au} (V)	500	500

Fabrication date: 13-04-2007

CMAFM date: -

ICMAFM date: 13-04-2007

A.5 10 mTorr samples March (CM only)

22-03 10mT (100.0)

	Pre-sputter	Sputter
P (mTorr)	10	10
Φ_{Ar} (ml/min)	25	25
Φ_{O_2} (ml/min)	0	0
f_{rotat} (Hz)	0.1	0.1
t_s (s)	30	90
I_s (mA)	100	100
U_{MoGe} (V)	295	307
U_{Au} (V)	441	449

Fabrication date: 22-03-2007

CMAFM date: 22-03-2007

ICMAFM date: -

22-03 10mT (90.10)

	Pre-sputter	Sputter
P (mTorr)	10	10
Φ_{Ar} (ml/min)	25	25
Φ_{O_2} (ml/min)	2.8	2.8
f_{rotat} (Hz)	0.1	0.1
t_s (s)	30	90
I_s (mA)	100	100
U_{MoGe} (V)	297	307
U_{Au} (V)	470	472

Fabrication date: 22-03-2007

CMAFM date: 22-03-2007

ICMAFM date: -

22-03 10mT (80.20)

	Pre-sputter	Sputter
P (mTorr)	10	10
Φ_{Ar} (ml/min)	25	25
Φ_{O_2} (ml/min)	6.3	6.3
f_{rotat} (Hz)	0.1	0.1
t_s (s)	30	90
I_s (mA)	100	100
U_{MoGe} (V)	296	307
U_{Au} (V)	495	495

Fabrication date: 22-03-2007

CMAFM date: 22-03-2007

ICMAFM date: -

22-03 10mT (70.30)

	Pre-sputter	Sputter
P (mTorr)	10	10
Φ_{Ar} (ml/min)	25	25
Φ_{O_2} (ml/min)	10.7	10.7
f_{rotat} (Hz)	0.1	0.1
t_s (s)	30	90
I_s (mA)	100	100
U_{MoGe} (V)	295	307
U_{Au} (V)	513	514

Fabrication date: 22-03-2007

CMAFM date: 22-03-2007

ICMAFM date: -

22-03 10mT (60.40)

	Pre-sputter	Sputter
P (mTorr)	10	10
Φ_{Ar} (ml/min)	25	25
Φ_{O_2} (ml/min)	16.7	16.7
f_{rotat} (Hz)	0.1	0.1
t_s (s)	30	90
I_s (mA)	100	100
U_{MoGe} (V)	296	307
U_{Au} (V)	528	530

Fabrication date: 22-03-2007

CMAFM date: 23-03-2007

ICMAFM date: -

22-03 10mT (50.50)

	Pre-sputter	Sputter
P (mTorr)	10	10
Φ_{Ar} (ml/min)	20	20
Φ_{O_2} (ml/min)	20	20
f_{rotat} (Hz)	0.1	0.1
t_s (s)	30	90
I_s (mA)	100	100
U_{MoGe} (V)	294	307
U_{Au} (V)	538	541

Fabrication date: 22-03-2007

CMAFM date: 23-03-2007

ICMAFM date: -

A.6 10 mTorr samples April

02-04 10mT (100.0)

	Pre-sputter	Sputter
P (mTorr)	10	10
Φ_{Ar} (ml/min)	25	25
Φ_{O_2} (ml/min)	0	0
f_{rotat} (Hz)	0.1	0.1
t_s (s)	30	90
I_s (mA)	100	100
U_{MoGe} (V)	298	306
U_{Au} (V)	435	435

Fabrication date: 02-04-2007

CMAFM date: 02-04-2007

(CMAFM images have tip artifacts)

First ICMAFM date: 04-04-2007

Second ICMAFM date: 13-04-2007

02-04 10mT (90.10)

	Pre-sputter	Sputter
P (mTorr)	10	10
Φ_{Ar} (ml/min)	25	25
Φ_{O_2} (ml/min)	2.8	2.8
f_{rotat} (Hz)	0.1	0.1
t_s (s)	30	90
I_s (mA)	100	100
U_{MoGe} (V)	292	306
U_{Au} (V)	466	466

Fabrication date: 02-04-2007

CMAFM date: 02-04-2007

(CMAFM images have tip artifacts)

First ICMAFM date: 04-04-2007

Second ICMAFM date: 13-04-2007

02-04 10mT (80.20)

	Pre-sputter	Sputter
P (mTorr)	10	10
Φ_{Ar} (ml/min)	25	25
Φ_{O_2} (ml/min)	6.3	6.3
f_{rotat} (Hz)	0.1	0.1
t_s (s)	30	90
I_s (mA)	100	100
U_{MoGe} (V)	293	306
U_{Au} (V)	490	490

Fabrication date: 02-04-2007

CMAFM date: 02-04-2007

(CMAFM images have tip artifacts)

First ICMAFM date: 04-04-2007

Second ICMAFM date: 13-04-2007

03-04 10mT (70.30)

	Pre-sputter	Sputter
P (mTorr)	10	10
Φ_{Ar} (ml/min)	25	25
Φ_{O_2} (ml/min)	10.7	10.7
f_{rotat} (Hz)	0.1	0.1
t_s (s)	30	90
I_s (mA)	100	100
U_{MoGe} (V)	292	306
U_{Au} (V)	509	509

Fabrication date: 03-04-2007

CMAFM date: 03-04-2007

(CMAFM images have tip artifacts)

First ICMAFM date: 04-04-2007

Second ICMAFM date: 13-04-2007

03-04 10mT (60.40)

	Pre-sputter	Sputter
P (mTorr)	10	10
Φ_{Ar} (ml/min)	25	25
Φ_{O_2} (ml/min)	16.7	16.7
f_{rotat} (Hz)	0.1	0.1
t_s (s)	30	90
I_s (mA)	100	100
U_{MoGe} (V)	292	306
U_{Au} (V)	523	524

Fabrication date: 03-04-2007

CMAFM date: 03-04-2007

(CMAFM images have tip artifacts)

First ICMAFM date: 04-04-2007

Second ICMAFM date: 13-04-2007

03-04 10mT (50.50)

	Pre-sputter	Sputter
P (mTorr)	10	10
Φ_{Ar} (ml/min)	20	20
Φ_{O_2} (ml/min)	20	20
f_{rotat} (Hz)	0.1	0.1
t_s (s)	30	90
I_s (mA)	100	100
U_{MoGe} (V)	292	306
U_{Au} (V)	534	536

Fabrication date: 03-04-2007

CMAFM date: 03-04-2007

(CMAFM images have tip artifacts)

First ICMAFM date: 04-04-2007

Second ICMAFM date: 13-04-2007

References

[1] D. A. Glocker and S. Ismat Shah, Thin Film Process Technology Volume 1, IOP Publishing, Ltd. (2002).

[2] M. Ohring, The Materials Science of Thin Films, Academic Press, (1992).

[3] S. A. Bashar Ph.D. thesis "Study of Indium Tin Oxide (ITO) for Novel Optoelectronic Devices" (1998).

[4] L. Fei Ph.D. thesis "Instrument Response Function for Scanning Force Microscopy and Defects on Mica Induced by 50 kilo-electron-volt argon ions" (1996).

[5] Digital Instruments, Veeco Metrology Group, "Scanning Probe Microscopy Training Notebook Version 3" (2000).

[6] L. Maya, C. E. Vallet, and Y. H. Lee, J. Vac. Sci. Technol. A **15**, 238 (1997).

[7] A. Bendavid, P. J. Martin and L. Wieczorek, Thin Solid Films **354**, 169 (1999).

[8] M. Tay, K. Li, and Y. Wu, J. Vac. Sci. Technol. B **23**, 1412 (2005).

[9] G. Binnig, H. Rohrer, Ch. Gerber, and E. Weibel, Phys. Rev. Lett. **49**, 57 (1982).

[10] G. Binnig, C. F. Quate and Ch. Gerber, Phys. Rev. Lett. **56**, 930 (1986).

[11] G. Binnig and D.P.E. Smith, Rev. Sci. Instrum. **57**, 1688 (1986).

[12] J. A. Venables, G. D. T. Spiller and M. Hanbücken, Rep. Prog. Phys. **47**, 399 (1984).

[13] I. Horcas, R. Fernandez, J.M. Gomez-Rodriguez, J. Colchero, J. Gomez-Herrero and A. M. Baro, Rev. Sci. Instrum. **78**, 013705 (2007).

[14] http://hyperphysics.phy-astr.gsu.edu/hbase/hframe.html

[15] http://research.memphis.edu/msr/

[16] http://en.wikipedia.org/

Acknowledgements

The work presented in this report has been done at the Kamerlingh Onnes Laboratory, Leiden Institute of Physics, Leiden University and in particular at the Magnetic and Superconducting Materials group. My thanks go out to:

- Prof. Dr. J. Aarts, for his supervision as head of the MSM group and also for the opportunity to complete my internship at the MSN group.
- Ing. R.W.A. Hendrikx, for his direct supervision and XRR measurements.
- Ing. M. Hesselberth, for his technical support.
- All the other members of the MSM group, who where always there to answer the simple questions.
- D.M. Paardekooper, for his useful discussions and comments.